

Functional Data Representation with Merge Trees

Matteo Pegoraro*, Piercesare Secchi †

November 11, 2024

Abstract

In this paper we face the problem of representation of functional data with the tools of algebraic topology. We represent functions by means of merge trees, which, like the more commonly used persistence diagrams, are invariant under homeomorphic reparametrizations of the functions they represent, thus allowing for a statistical analysis which is indifferent to functional misalignment. We consider a recently defined metric for merge trees and we prove some theoretical results related to its specific implementation when merge trees represent functions, establishing also a class of consistent estimators with convergence rates. To showcase the good properties of our topological approach to functional data analysis, we test it on the Aneurisk65 dataset replicating, from our different perspective, the supervised classification analysis which contributed to make this dataset a benchmark for methods dealing with misaligned functional data. In the Appendix we provide an extensive comparison between merge trees and persistence diagrams, highlighting similarities and differences, which can guide the analyst in choosing between the two representations.

Keywords: Topological Data Analysis, Functional Alignment, Merge Trees, Tree Edit Distance, Stability, Consistent Estimators

1. Introduction

Since the publication of the seminal books by Ramsay and Silverman (Ramsay and Silverman, 2005) and Ferraty and Vieu (Ferraty and Vieu, 2006), Functional Data Analysis (FDA) has become a staple of researchers dealing with data where each statistical unit is represented by the measurements of a real random variable observed on a grid of points belonging to a continuous, often one dimensional, domain D . In FDA these individual data are better represented as the sampled values of a function defined on D and with values in \mathbb{R} . Hence, at the onset of any particular functional data analysis stands the three-faceted problem of *representation*, described by: (1) the smoothing of the raw and discrete individual data to obtain a functional descriptor of each unit in the data set, (2) the identification of a suitable embedding space for the sample of functional data thus obtained and, finally, (3) the eventual alignment of these functional data consistently with the structure of the embedding space. As a reference benchmark of the typical FDA pipeline applied to a real world dataset, we take the paper by Sangalli et al. (2009b) where the first functional data analysis of the AneuRisk65 dataset is illustrated.

Smoothing is the first step of a functional data analysis. For each statistical unit, individual raw data come in the form of a discrete set of observations regarded as partial observations of a function. Smoothing is the process by means of which the analyst generates the individual functional object out of the raw data. This functional object

*. Department of Mathematical Sciences, Aalborg University

†. MOX, Department of Mathematics, Politecnico di Milano

will be the atom of the subsequent analysis, a point of a functional space whose structure is apt to sustain the statistical analysis required by the problem at hand. Commons approaches to obtain functional representations are to employ kernel estimators (Nadaraya, 1964; Schuster and Yakowitz, 1979; Müller, 1984; Mack and Müller, 1989) or to fit the data with a member of a finite dimensional functional space generated by some basis, for instance, splines or trigonometric polynomials. Signal-to-noise ratio and the degree of differentiability required for the functional representation, as well as the structure of the embedding space, drive the smoothing process. Functional representations interpolating the raw data are of no practical use when the analysis requires to consider functions and their derivatives or, for instance, the natural embedding space is Sobolev's; see, for instance, Sangalli et al. (2009a) for a detailed analysis of the trade-off between goodness of fit and smoothness of the functional representation when dealing with the Aneurisk65 dataset.

Functional data express different types of variability (Vantini, 2009) which the analyst might want to decouple before carrying out the statistical analysis. Indeed the Aneurisk65 dataset is by now considered a benchmark for methods aimed at the identification of *phase* and *amplitude variation* (see the Special Section on Time Warpings and Phase Variation on the Electronic Journal of Statistics, Vol 8 (2), and references therein). In many applications phase variation captures ancillary non-informative variability which could alter the results of the analysis if not properly taken into account (Lavine and Workman, 2008; Marron et al., 2014). A common approach to this issue is to embed the functional data in an appropriate Hilbert space where equivalence classes are defined, based on a notion of *alignment* or *registration*, and then to look for the most suitable representative for any of these classes (Marron et al., 2015). Such approach evokes ideas from shape analysis (Dryden and Mardia, 1998) and pattern theory (Grenander, 1993), where configurations of landmark points are identified up to rigid transformations and global re-scalings. In close analogy with what has been done for curves (Michor et al., 2007; Srivastava et al., 2011b), functions defined on compact real intervals D are aligned by means of warping functions mapping D into another interval; that is, functional data are identified up to some re-parametrization. Different kinds of warping functions have been investigated: affine warpings are studied for instance in Sangalli et al. (2010) while more general diffeomorphic warpings have been introduced in Srivastava et al. (2011a). Once the *best* representatives are selected, the analysis is carried out on them leveraging the well behaved Hilbert structure of the embedding space. Classically, the optimal representatives are found by minimizing some loss criterion with carefully studied properties (Sangalli et al., 2014). This approach however has some limitations, arising from the fact that the metric structure of the embedding space might not be compatible with the equivalence classes collecting aligned functions (Yu et al., 2013). An alternative is to employ metrics directly defined on equivalence classes of functions such as the Fisher Rao metric, originally introduced for probability densities (Srivastava et al., 2007), which allows for the introduction of diffeomorphic warpings (Srivastava et al., 2011a). It must be pointed out that all these ways of dealing with the issue of ancillary phase variability encounter some serious challenges when the domain D is not a compact real interval.

A different approach to the problem of phase variation is to capture the information content provided by a functional datum by means of a statistic which is insensitive to the function re-parametrization, but sufficient for the analysis. Algebraic topology can help since it provides tools for identifying information which is invariant to deformations of a given topological space (Hatcher, 2000). Topological Data Analysis (TDA) is a quite recent field in data analysis and consists of different methods and algorithms whose foundations

rely on the theory developed by algebraic topology (Edelsbrunner and Harer, 2008). The main source of information collected by TDA algorithms are homology groups (see, for instance, Hatcher (2000)) with fields coefficients which, roughly speaking, count the number of holes (of different kinds) in a topological space. For instance zero dimensional holes are given by path connected components and one dimensional holes are given by classes of loops (up to continuous deformations) which cannot be shrunk to one point. One of the most interesting and effective ideas in TDA is that of *persistent homology* (Edelsbrunner et al., 2002): instead of fixing a topological space and extracting the homology groups from that space, a sequence of topological spaces is obtained along various pipelines, and the evolution of the homology groups is tracked along this sequence. The available pipelines are many, but the one which is most interesting for the purposes of this work is that concerning real valued functions. Let the domain D be a topological space X and consider a real valued function defined on X , $f : X \rightarrow \mathbb{R}$. One can associate to f the sequence of topological spaces given by the sublevel sets $X_t = f^{-1}((-\infty, t])$, with t ranging in \mathbb{R} . The evolution of the connected components along $\{X_t\}_{t \in \mathbb{R}}$ is thus analysed for the purpose of generating a topological representation of f . In this work, we consider specific topological representations of f constructed along this general scheme, and invariant with respect to homeomorphic warpings of the domain X . This two property makes the TDA approach pursued in this manuscript a candidate for the representation of functional data, indeed a robust competitor able to deal in a natural way with phase variation.

To allow for the statistical analysis of functional data summarised by their topological representations, we need to embed the latter in a metric space. The choice of persistence diagrams (PD) (Cohen-Steiner et al., 2007) as summaries obtained through persistent homology drives many successful applications (Xia et al., 2018; Bhattacharya et al., 2015; Pokorny et al., 2016; Chung et al., 2009; Wang et al., 2018; Kramár et al., 2013), although other topological summaries are in fact known in the literature (Bubenik, 2015; Adams et al., 2017; Chazal et al., 2015). In this work we exploit a topological alternative – not equivalent – to a persistence diagram, called *merge tree*. Merge trees representations of functions are not new (Morozov and Weber, 2013) and are obtained as a particular case of Reeb Graphs (Shinagawa et al., 1991; Biasotti et al., 2008). Different frameworks have been proposed to work with merge trees (Beketayev et al., 2014; Morozov et al., 2013), mainly defining a suitable metric structure to compare them (Gasparovic et al., 2019; Touli, 2020). However all such metrics have a very high computational cost, causing a lack of examples and applications even when approximation algorithms are available (Touli and Wang, 2019), or they require complex workarounds to be effectively used (Sridharamurthy et al., 2020). We employ the metric for merge trees introduced in Pegoraro (2024a), showing that its computational complexity is reasonable when the trees involved are not too large.

Contributions

When working with representations of data, it is fundamental to study the behaviour of the operator which maps the single datum into the chosen representation to assess which kind of information is transferred from the initial data to the space of representations. For this reason we highlight the invariance properties of the chosen representation and develop a new theoretical analysis on the stability/continuity of merge trees with respect to perturbations of the original functions. This fundamental result is also used to prove other important properties, with which we build consistent estimators of merge trees obtained from functions observed on a grid up to some noise. We point out that in Pegoraro (2024a) it is proven that the stability properties we establish here are in line with the most used

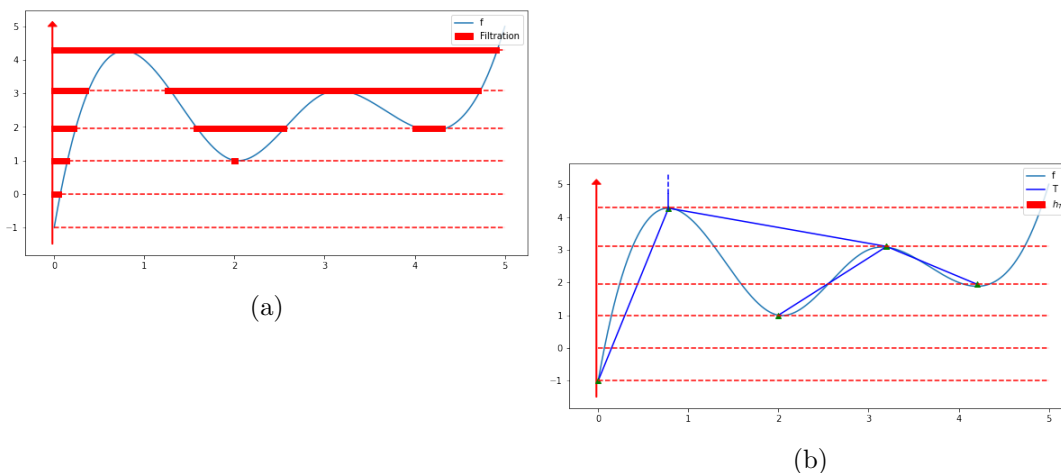


Figure 1: Sublevel sets of a function (a); the same function with its associated merge tree (b).

family of distances between persistence diagrams, namely they are analogous to the ones of the 1-Wasserstein distance.

Outline

The paper is organized as follows. In Section 2, we introduce the merge tree representation of a function and the metric structure for the space of merge trees which is used in the examples and in the final case study. In Section 3 we briefly recall the definition of persistence diagrams in order to draw some comparison between them and merge trees, before turning to the invariance property, which holds true for both topological representations. Section 4 contains the main theoretic investigations of the paper with results dealing with a) the continuity properties of the operator which assigns to a function its merge tree, with respect to the aforementioned metric; b) the problem of consistently estimating merge trees from samples; c) the problem of the computational approximation of merge trees. In Section 5, we tackle the functional data classification problem explored in Sangalli et al. (2009b) and we compare their results with those obtained following the TDA approach we advocate in this paper. We finally conclude the manuscript with a discussion, in Section 7, which points out some ideas pertaining to our topological approach to functional data analysis.

Appendix A contains additional figures and tables which can help the reader throughout the manuscript. While Appendix B develops a detailed discussion on how merge trees can be obtained in more general scenarios w.r.t the one considered in the main manuscript. Then, in Appendix C, we propose some *in silico* examples to further illustrate differences and similarities between persistence diagrams and merge trees.

Lastly, Appendix D collects the proofs of the results of the paper.

2. Merge Trees of Functions

2.1 Sublevel Sets

In the upcoming sections we define the merge tree representation of a function. Merge trees are an already established tool in topology and, to some extent, also in statistics since dendrograms can be regarded as merge trees. Nevertheless, we are going to spend

a few lines to define them, in accordance with the framework of Pegoraro (2024a), which differs from the classical one, found, for instance, in Morozov and Weber (2013). Roughly speaking, the pipeline to obtain a merge tree is the following: we transform the given function into a sequence of nested subsets and then we track the topological changes along this sequence. Such information is then turned into a tree.

Consider a function $f : X \rightarrow \mathbb{R}$, with X being any topological space. We call sublevel set at height $t \in \mathbb{R}$, the set $X_t := f^{-1}((-\infty, t]) \subset X$. The key property of the family $\{X_t\}_{t \in \mathbb{R}}$ is that such subsets are nested: if $t \leq t'$ then $X_t \subset X_{t'}$. Note that the sequence $\{X_t\}_{t \in \mathbb{R}}$ is fully determined by the shape of the function f ; see Figure 1a. In fact, for $x \in X$, $f(x) = \inf\{t \in \mathbb{R} : x \in X_t\}$, hence no information carried by f is lost by its representation $\{X_t\}_{t \in \mathbb{R}}$.

2.2 Path Connected Components

A topological space X is path connected if for every couple of points $x, y \in X$ there is a continuous curve $\alpha : [0, 1] \rightarrow X$ such that $\alpha(0) = x$ and $\alpha(1) = y$. The biggest path connected subsets contained in a topological space are called path-connected components.

The covariant functor (Mac Lane, 1998) of path-connected components is usually referred to as π_0 , meaning that, given a topological space X , $\pi_0(X)$ is the set of the path connected components of X . If $q : X \rightarrow Y$ is a continuous function between two topological spaces X and Y , one can define the function $\pi_0(q) : \pi_0(X) \rightarrow \pi_0(Y)$ as follows: $U \mapsto V$ if $q(U) \subset V$.

Being a functor, π_0 satisfies a number of properties. Among them, we emphasize the following: for two continuous functions p, q that can be composed into the function $p \circ q$, it is true that $\pi_0(p \circ q) = \pi_0(p) \circ \pi_0(q)$.

Path-connected components are the source of information we want to track along the family $\{X_t\}_{t \in \mathbb{R}}$. For $t \in \mathbb{R}$, let $\pi_0(X_t) = \{U_i^t\}_{i \in I}$ be the set of the path-connected components of X_t and consider $f : X \rightarrow \mathbb{R}$ continuous. By definition the sets X_t are closed subsets of X , and the inclusions $i_t^{t'} : X_t \hookrightarrow X_{t'}$ are continuous maps. In this way we can induce $\pi_0(i_t^{t'}) : \pi_0(X_t) \rightarrow \pi_0(X_{t'})$ such that $U_i^t \subset \pi_0(i_t^{t'})(U_i^t)$ for all $U_i^t \in \pi_0(X_t)$.

2.3 Assumptions on $f : X \rightarrow \mathbb{R}$

In this manuscript we have two major sets of hypotheses that we want to consider: a more general one, which however requires a series of technicalities that interfere with the flow of the discussion; and a set of simplified assumptions which decrease significantly the work needed to introduce some of the upcoming constructions. We now introduce the sets of assumptions, splitting also the general one into two sub-cases, and comment on them.

To avoid ambiguities we recall the following notation: x is an isolated minimum (point) for f if $f(y) > f(x)$ on some open neighborhood of x . Similarly, x is an isolated maximum (point) for f if $f(y) < f(x)$ on some open neighborhood of x .

These are the sets of assumptions we consider:

- (A0) $f : X \rightarrow \mathbb{R}$ is a *tame* (see Chazal et al. (2016) or the appendix) function on a path connected topological space X ;
- (A1) $f : X \rightarrow \mathbb{R}$ is a *tame* (see Chazal et al. (2016) or the appendix) continuous function on a path connected topological space X ;
- (B) $f : X \rightarrow \mathbb{R}$ is a continuous function presenting only a finite number of local maxima and minima points (which therefore are isolated), with $X = [a, b] \subset \mathbb{R}$ being a compact real interval.

Note that if f satisfies (B), then it also satisfies (A1) and (A0). Clearly (A1) implies (A0).

The general idea which we follow in this manuscript is to state and discuss everything using assumptions (B), to avoid overloading the reader with notation and technicalities, and introducing our novelties in a more familiar setting. However, 1) we still report in the appendix definitions and constructions allowing to build merge trees under assumptions (A0) 2) Theorem 6, Theorem 11 and Theorem 12 are stated and assuming (A0) and (A1) so that they are available in full generality. In particular, assuming (A0) and (A1) instead of (B) does not require any relevant changes in the proofs. On a similar note, we point out that the results in Section 4.2 and Section 4.3 have been proven only for functions satisfying (B).

2.4 Tree Structures, Critical Values and Topological Changes

Coherently with Pegoraro (2024a), we now define what we mean with *tree* and with *merge tree*.

Definition 1 *A tree structure T is given by a set of vertices V_T and a set of edges $E_T \subset V_T \times V_T$ which form a connected rooted acyclic graph. We indicate the root of the tree with r_T . We say that T is finite if V_T is finite. The order of a vertex of T is the number of edges which have that vertex as one of the extremes. Any vertex with an edge connecting it to the root is its child and the root is its father: this is the first step of a recursion which defines the father and children relationship for all vertices in V_T . The vertices with no children are called leaves or taxa. The relation child $<$ father generates a partial order on V_T . The edges in E_T are identified in the form of ordered couples (v, w) with $v < w$. A subtree of a vertex v is the tree structure whose set of vertices is $\{x \in V_T | x \leq v\}$.*

Definition 2 (Gasparovic et al. (2019), Pegoraro (2024b)) *A finite tree structure T such that r_T is of order 1, coupled with a monotone increasing height function $h_T : V_T \rightarrow \mathbb{R} \cup \{+\infty\}$ with $h_T(r_T) = +\infty$ and $h_T(v) \in \mathbb{R}$ if $v < r_T$, is called merge tree.*

The heuristic idea behind the construction of the merge tree representation of $f : X \rightarrow \mathbb{R}$ is that, since along the sequence $\{X_t\}_{t \in \mathbb{R}}$ the path-connected components of X_t can only arise, merge with others, or stay the same, it is natural to represent this merging structure with a tree structure T . However, this tree T would not encode the values of the function at which these changes happen, hence we enrich it by defining a monotone increasing height function $h_T : V_T \rightarrow \mathbb{R} \cup \{+\infty\}$ encoding them. The reader may look at Figure 1b to have a visual interpretation of the construction. The height function is given by the dotted red lines.

We work under assumptions (B), and so the *critical values* of f are the values of f at its isolated maxima and minima points. We may refer to such local maxima and minima points as the critical points of the function. We recall that X , the domain of f , is some compact real interval $[a, b]$. Critical values admit a more general definition, which we report in the appendix, and which plays a central role in the construction of merge trees.

As also made clear by Figure 1b, local maxima and minima points of f are where the connectivity of the sublevel sets changes: at local minima we have the birth of new path connected components, while at local maxima we have the merging of two path connected components. In particular, local minima points will be associated to the leaves of the merge tree, while local maxima points to the internal vertices; the height of internal vertices and leaves is given by the respective critical values of f . Roughly speaking, the edges then

describe the merging pattern of the path connected components along the sublevel sets, connecting the critical points and values in the graph of f , as in Figure 1b.

Let $\{t_1, \dots, t_n\}$ be the critical values of f , listed in increasing order. The tree structure T and the height function h_T are built along the following rules, in a recursive fashion starting from an empty set of vertices V_T and an empty set of edges E_T . We simultaneously add points and edges to T and define h_T on the newly added vertices. From now on, we indicate with $\#C$ the cardinality of a finite set C .

- For the critical value t_1 add to V_T a leaf $v_{U_{t_1}}$, with height t_1 , for every element $U_{t_1} \in \pi_0(X_{t_1})$. These vertices correspond to the global minima points of f ;
- for t_i with $i > 1$, we add a leaf with height t_i for each local minimum point of f with value t_i . More formally, for every $U_{t_i} \in \pi_0(X_{t_i})$ such that $U_{t_i} \notin \text{Im}(\pi_0(i_{t_{i-1}}^{t_i}))$, add to V_T a leaf $v_{U_{t_i}}$ with height t_i ;
- similarly, for t_i with $i > 1$, we add an internal vertex with height t_i for each local maximum point of f with value t_i , connecting the path-connected components that merge at each local maximum. That is, if $U_{t_i} = \pi_0(i_{t_{i-1}}^{t_i})(U_{t_{i-1}}) = \pi_0(i_{t_{i-1}}^{t_i})(U'_{t_{i-1}})$, with $U_{t_{i-1}}$ and $U'_{t_{i-1}}$ distinct path connected components in $\pi_0(X_{t_{i-1}})$, add a vertex $v_{U_{t_i}}$ with height t_i , and add edges so that we connect the newly added vertex $v_{U_{t_i}}$ with each of the following previously added vertices :

$$v = \arg \max\{h_T(v'_U) \mid v'_U \in V_T \text{ s.t. } U \subset U_{i-1}\}$$

$$w = \arg \max\{h_T(w'_U) \mid w'_U \in V_T \text{ s.t. } U \subset U'_{i-1}\}.$$

The last merging happens at height t_n and, since X is path connected, at height t_n there is only one point v_U . Thus we can add a vertex r_T and an edge (v_U, r_T) with $h_T(r_T) = +\infty$ to obtain a merge tree. Looking at Figure 1b, we can appreciate that the merge tree of f is heavily dependent on the shape of f , in particular on the displacement of its maxima and minima points.

2.5 Isomorphism classes

If we change the parametrization of a function f by considering $g = f \circ \eta$, with η being an homeomorphism, the path-connected components of $f^{-1}(t)$ and $g^{-1}(t)$ will in general be different sets. Since the vertex sets of the merge trees of f and g are obtained from the path-connected components of sublevel sets, this implies that, to obtain invariance properties, we must consider merge trees up to relabeling of their vertices. In other words, as in Pegoraro (2024b) and Pegoraro (2024a), we don't want to distinguish trees if they differ just by the names of their vertices.

Definition 3 *Two tree structures T and T' are isomorphic if there exists a bijection $\eta : V_T \rightarrow V_{T'}$ inducing a bijection between the edges sets E_T and $E_{T'}$: $(v, w) \mapsto (\eta(v), \eta(w))$. Such η is an isomorphism of tree structures.*

Definition 4 *Two merge trees (T, h_T) and $(T', h_{T'})$ are isomorphic if T and T' are isomorphic as tree structures and the isomorphism $\eta : V_T \rightarrow V_{T'}$ is such that $h_T = h_{T'} \circ \eta$. Such η is an isomorphism of merge trees.*

2.6 Height and Weight Functions

A final step is needed to complete the specific representation of merge trees needed for making use of the metric defined in Pegoraro (2024a). The height function h_T of a generic merge tree T takes values in \mathbb{R} , but this is not an *editable* space, according to the definition in Pegoraro (2023), which we report here.

Definition 5 *Let W be a set endowed with a metric d and an associative operation $*$ with zero element $0 \in W$. Then $(W, d, *, 0)$ is said to be an editable space if the following two properties are both satisfied:*

(P1) *the map $d(\cdot, 0) : W \rightarrow \mathbb{R}$ is a map of monoids between $(W, *)$ and $(\mathbb{R}, +)$, that is:*
 $d(x * y, 0) = d(x, 0) + d(y, 0)$ *for all $x, y \in W$;*

(P2) *d is $*$ invariant, that is: $d(x, y) = d(z * x, z * y) = d(x * z, y * z)$ for all $x, y, z \in W$.*

Note that, whereas \mathbb{R} is not editable because $|x + (-x)| \neq |x| + |-x|$, $\mathbb{R}_{\geq 0}$ is editable. Thus, what we roughly need to do is to turn each merge tree into a positively weighted tree, via some careful transformation. Consequently, we complement the merge tree T with a transformation of the height function h_T : a weight function w_T defined on $V_T - \{r_T\}$ whose image is a subset of the editable space $\mathbb{R}_{\geq 0}$. To do so, as in Pegoraro (2024a), we employ a truncation strategy which takes care of the edge (v, r_T) which goes at infinity. Such strategy relies on the following assumption.

Assumption 1 *We assume the existence of a universal constant $K \in \mathbb{R}$ bounding above all the functions for which we will adopt a merge tree representation.*

In Pegoraro (2024a) it is shown that all the upcoming steps in the construction of the specific merge trees considered in this paper, do not depend on K , in the sense that with any $K' > K$ we would obtain the same results. We spend some more words on this issue in the following Theorem 9.

Given a merge tree (T, h_T) , as a first step we define the function $h'_T : V_T \rightarrow \mathbb{R}$ as $h'_T(v) = h_T(v)$ for all $v < r_T$ and $h'_T(r_T) = K$. Then for every vertex $v \in V_T - \{r_T\}$, we consider the unique edge between v and its father w and we define $w_T(v) = h'_T(w) - h'_T(v)$; the weight function w_T also codes the weight of the edge (v, w) , via the rule $w_T((v, w)) = w_T(v)$, which identifies the set of edges E_T with vertices in $V_T - \{r_T\}$. Note that, because of Assumption 1, there is a one-to-one correspondence between h_T and w_T . Finally, the monotonicity of h_T and Assumption 1 guarantee that $w_T(v) \in \mathbb{R}_{\geq 0}$, for all $v \in V_T - \{r_T\}$. See Figure 2 for a visual example.

The height function introduced in Theorem 2 turns out to be quite natural for the definition of a merge tree, but from now on along with the height function h_T we also employ the induced weight functions w_T .

2.7 Properties

In this section we state the invariance property anticipated in the introduction and we also point out a few differences between persistence diagrams and merge trees.

Proposition 6 (Invariance) *The isomorphism class of the merge tree of a function $f : X \rightarrow \mathbb{R}$ satisfying (A0), is invariant under homeomorphic re-parametrization of f .*

Remark 7 *As an immediate consequence of Theorem 6 we obtain that, if the functions f and g can be aligned by means of a homeomorphism, that is if $f = g \circ \eta$ being η an homeomorphism, then their associated merge trees T_f and T_g are isomorphic.*

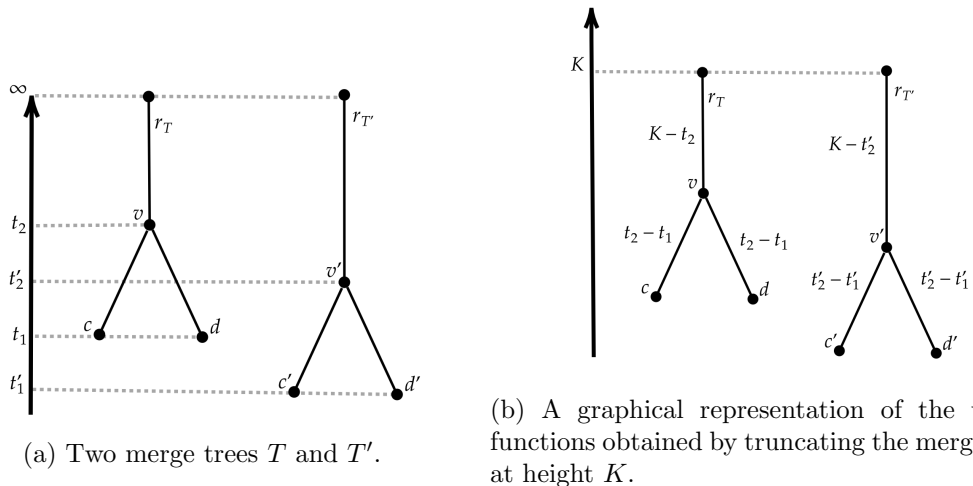


Figure 2: A graphical representation of the truncation process described in Section 2.6.

In other words, we can warp, deform, move the domain X of a function f by means of any homeomorphism, and this will have no effect on its associated merge tree. As a consequence, if each element of a sample of functions is represented by its merge tree, one can carry out the statistical analysis without worrying about possible misalignments, that is without first singling out, for each function of the sample, the specific warping function, identified by an homeomorphism, which decouples its phase and amplitude variabilities.

2.8 The Metric for Merge Trees

The metric for weighted graphs defined in Pegoraro (2023) and then adapted to merge trees in Pegoraro (2024a) is based on edit distances (Bille, 2005; Hong et al., 2017): they allow for modifications of a starting object, each with its own cost, to obtain a second object. Merge trees equipped with their weight function w_T , as defined in Section 2.6, fit into this framework; hence the space of merge trees can be endowed with a metric based on an edit distance and called d_E in the following.

The distance d_E is very different from previously defined edit distances, since it is specifically designed for comparing topological summaries, roughly meaning that all points which are topologically irrelevant can be eliminated by a merge tree without paying any cost. To make things more formal we here introduce the edits, as defined in Pegoraro (2024a).

The edits are the followings and can be used to modify any edge (v, v') of a merge tree, or equivalently its lower vertex v :

- *shrinking* an edge means changing the weight value of the edge with a new positive value. The inverse of this transformation is the shrinking which restores the original edge weight.
- *Deleting* an edge (v_1, v_2) results into a new tree, with the same vertices apart from v_1 (the lower one), and with the father of the deleted vertex which gains all of its children. With a slight abuse of language, we might also refer to this edit as the deletion of the vertex v_1 , which indeed means deleting the edge between v_1 and its father.

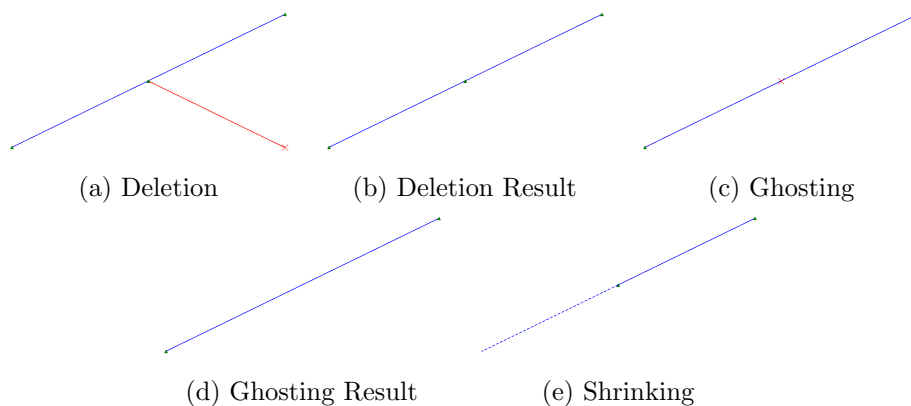


Figure 3: (a)→(e) form an edit path made by one deletion, one ghosting and a final shrinking.

The inverse of deletion is the *insertion* of an edge along with its child vertex. We can insert an edge at a vertex v specifying the child of v and its children (that can be either none or any portion of the children of v) and the weight of the edge.

- Lastly, we can eliminate an order two vertex v , that is a father with an only child, connecting the two adjacent edges which arrive and depart from v . The weight of the resulting edge is the sum of the weights of the joined edges. This transformation is the *ghosting* of the vertex v . Its inverse transformation is called the *splitting* of an edge.

The costs of the edit operations are defined as follows:

- the cost of shrinking an edge is equal to the absolute value of the difference of the two weights;
- for any deletion/insertion, the cost is equal to the weight of the edge deleted/inserted;
- the cost of ghosting is zero.

Given a tree T we can edit it, thus obtaining another tree, on which we can apply a new edit to obtain a third tree and so on. Any finite composition of edits is called an *edit path*. The cost of an edit path is the sum of the costs of its edit operations. Putting all the pieces together, we can define the edit distance d_E as:

$$d_E(T, T') = \inf_{\gamma \in \Gamma(T, T')} \text{cost}(\gamma)$$

where $\Gamma(T, T')$ indicates the set of edit paths which start in T and end in T' .

Remark 8 *Edit operations are not globally defined as operators mapping merge trees into merge trees. They are defined on the individual tree. Similarly, their inverse is not the inverse in the sense of operators, but it indicates that any time we travel from a tree T to a tree T' by making a sequence of edits, we can also travel the inverse path going from T' to T and restore the original tree.*

Remark 9 *The results in Pegoraro (2024a) show that the metric $d_E(T, T')$ does not depend on the value of K used in the truncation process and introduced with Assumption*

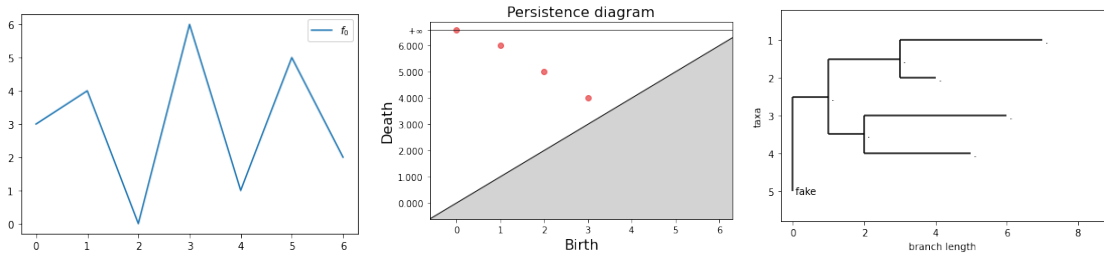


Figure 4: A function (left) with its associated persistence diagram (centre) and merge tree (right). On the PD axes we see the birth and death coordinates of its points. The plot of the merge tree features the length of its branches (given by the weight function - Section 2.6) on the horizontal axis, and the leaves (taxa) are displaced on the vertical axis. The vertical axis scale is only for visualization purposes. The merge tree is truncated at height 7 - see Section 2.6.

1. *To be sure, if, after having fixed K to analyze a set of merge trees \mathcal{T} , we add to the set a new merge tree corresponding to a function f which is not bounded above by K , we proceed by fixing a novel K' bounding f and all the other functions represented in the set \mathcal{T} , and compute $d_E(T_f, T_g)$, for all $g \in \mathcal{T}$, after truncating all merge trees in $\mathcal{T} \cup \{T_f\}$ at height K' . This won't affect the distances between merge trees in \mathcal{T} computed before the addition of T_f , when the truncation constant was K , since the metric d_E is the same for such merge trees. Thus Assumption 1 is in some sense unnecessary, since we do not need to fix K uniformly on our data set but only in a pairwise fashion. However for our applications such assumption is never violated, so we can assume it and avoid some formal complications arising from having to fix K for every couple of functions.*

Remark 10 *The null cost of ghosting guarantees that order 2 vertices are completely irrelevant when computing the cost of an edit path. In Pegoraro (2024b) it is proved that d_E is a metric on the space of merge trees, identified up to order 2 vertices. As explained in Pegoraro (2024b), the fact that order 2 vertices are irrelevant is precisely what makes the metric d_E suitable for comparing merge trees and is fundamental to obtain the results in Section 4.*

3. Persistence Diagrams

Persistence diagrams are arguably among the most well known tools of TDA; for a detailed survey see, for instance, (Edelsbrunner and Harer, 2008). We here briefly introduce persistence diagrams since in the following sections we use them to draw comparisons with merge trees.

Loosely speaking a persistence diagram is a collection of points (c_x, c_y) in the first quadrant of \mathbb{R}^2 , with $c_y > c_x$ and such that: c_x is the t corresponding to the first appearance of an homology class in X_t (birth), while c_y is the t where the same class merges with a different class appeared before c_x (death). Homology classes are a generalization of path-connected components to “holes in higher dimension”; path-connected components can be seen as zero dimensional holes. For more details see Hatcher (2000).

In this work we focus on persistence diagrams associated to path-connected components, since we want to compare them with the merge trees introduced in the previous section. Given a function $f : X \rightarrow \mathbb{R}$, we associate to f the zero dimensional persistence diagram $(PD(f))$ of the sequence of sublevel sets $\{X_t\}_{t \in \mathbb{R}}$. We highlight that, in such rep-

resentation, there is no information about which path-connected component merges with which; in fact a component represented by the point (c_x, c_y) , at height c_y could merge with any of the earlier born and “still alive” components. Of course this collection of points still depends on the shape of the function and in particular depends on its amplitude and the number of its oscillations. See Figure 4. Note that, while for merge trees one needs to be careful and consider appropriate isomorphism classes so that the representation does not depend, for instance, on the names chosen for the vertices (that is, the set V_T), this issue does not appear with persistence diagrams. Topological features are represented as points in the plane, without labels or other kinds of set-dependent information. Thus, two persistence diagrams are isomorphic if and only if they are made of the same set of points.

We point out that the equivalence classes of isomorphic merge trees generated by Theorem 4 are coherent with what happens with persistence diagrams, where no specific information about individual path connected components (size, shape, position, the actual points contained etc.) is retained.

3.1 Properties

Proposition 11 *For all $f : X \rightarrow \mathbb{R}$ satisfying (A0), the associated PD(f) in dimension 0 can be obtained from the associated merge tree T_f .*

Thus, if two functions induce isomorphic merge trees, they also have the same persistence diagrams. Which also implies that PDs also satisfy the invariance property.

Despite sharing this important invariance property, a persistence diagram and a merge tree are not equivalent representations of a function. Indeed, persistence diagrams do not record information about the merging components: as already mentioned, the death of a path connected component could be caused by its merging with any other alive component at death-time. This implies that, for a given persistence diagram PD, there might be more than one merge tree associated to the diagram: the birth and death of the path connected components of each merge tree coincide with those of the PD, but the merging structure is different from merge tree to merge tree (Kanari et al., 2020; Curry et al., 2021; Pegoraro, 2024b; Curry et al., 2022; Elkin and Kurlin, 2020; Smith and Kurlin, 2022). In particular, the works of Kanari et al. (2020) and of Curry et al. (2021) formally address this point, by providing explicit formulas for the *tree realization number*: the number of trees associated to the same persistence diagram. This number can be very high, being $n!$ if n is the number of points in the diagram, for certain configurations of the persistent diagram. This is the case, for instance, with hierarchical clustering dendrograms with n leaves: all leaves are born at height 0, and so, at the first merging point, each of the n leaves can merge with any of the $n - 1$ remaining ones. At the following merging step we have $n - 1$ clusters and each one of them can merge with the other $n - 2$ and so on. Thus, depending on the structure of the persistence diagram representing a function f , the associated merge tree could contain much more information regarding f ; from a different perspective, merge trees can discriminate between functions which are indistinguishable for persistent diagrams. To see some easy examples of how merge trees capture also the local merging structure of the components which persistent diagrams cannot distinguish, see Figure 6 in the appendix and Appendix C. Further details and insights on the differences between PDs and merge trees can also be found in Appendix C.

3.2 Metrics for Persistence Diagrams

The space of persistence diagrams can be given a metric structure by means of a family of metrics which derives from Wasserstein distances for bivariate distributions.

Given two diagrams D_1 and D_2 , the expression of such metrics is the following:

$$W_p(D_1, D_2) = \left(\inf_{\gamma} \sum_{x \in D_1} \|x - \gamma(x)\|_{\infty}^p \right)^{1/p}$$

where $p \geq 1$ and γ ranges over the functions partially matching points between diagrams D_1 and D_2 , and matching the remaining points of both diagrams with the line $y = x$ on the plane (for details see Cohen-Steiner et al. (2007)). In other words we measure the distances between the points of the two diagrams, pairing each point of a diagram either with a point on the other diagram, or with a point on $y = x$. Each point can be matched once and only once. The minimal cost of such matching provides the distance.

4. Stability, Estimators and Approximations

4.1 Stability

As stated in the introduction of the paper, any time we use a data representation – or we further transform a representation – it is important to understand and explore the properties of the operators involved. In particular, in this section we want to establish some continuity properties for the operator $f \mapsto T_f$, which maps a function to its merge tree. Conditional on the topology endowing the functional space where the function f is embedded, these properties dictate how the variability between functions is captured by the variability between their merge tree representations.

Theorem 6 implies that the merge tree representation of a function f is unaffected by a large class of warpings of its domain, which would strongly perturb f if it was embedded, for instance, in an L_p space, with $p \neq \infty$. As an example, if $f : \mathbb{R} \rightarrow \mathbb{R}$ is bounded with compact support, shrinking f by setting $f_n(x) = f(x \cdot \lambda_n)$ with $\lambda_n \rightarrow +\infty$, produces no effect on the merge tree representation of f since $T_{f_n} = T_f$, while the p -norm of f_n goes to zero.

It might therefore be more natural to study the behavior of $f \mapsto T_f$ endowing the space of functions $f : X \rightarrow \mathbb{R}$ with the topology of uniform convergence, which captures pointwise closeness between functions. This topology, available for any domain X , has also the advantage of showing the effect of pointwise noise on merge tree representations. For these reasons, stability results in TDA are often stated via the sup norm of functions.

The main result of this section is the following.

Theorem 12 *Let $f, g : \mathbb{R} \rightarrow \mathbb{R}$ be functions satisfying (A1) and such that*

$$\sup_{x \in X} |f(x) - g(x)| \leq \varepsilon.$$

Let T_f and T_g be the merge trees associated to f and g respectively and let $N_f = \#V_{T_f}$ and $M_g = \#V_{T_g}$.

Then, there exists an edit path $e_1 \circ \dots \circ e_{N_f + M_g} \in \Gamma(T_f, T_g)$ which edits each vertex at most once and such that $\text{cost}(e_i) < 2 \cdot \varepsilon$, for $i = 1, \dots, N_f + M_g$.

Theorem 12 states that if two functions are pointwise close, then we can turn the merge tree associated to the first function into the merge tree associated to the second function using at most one edit per vertex, and each edit has a small cost. Note, however, that if the two functions have a very high number of oscillations, the distance between their merge trees could still be large. Indeed if $\|f_n - f\|_{\infty} \xrightarrow{n} 0$ we are not guaranteed

that $d_E(T_f, T_{f_n}) \rightarrow 0$. Theorem 12 however implies that, if the cardinalities $\#V_{T_{f_n}}$ are bounded, then $d_E(T_f, T_{f_n})$ indeed goes to 0. Lastly, we point out that in Pegoraro (2024a) it is shown that the widely used Wasserstein metrics between persistence diagrams satisfy stability properties analogous to the ones considered in Theorem 12.

4.2 Merge Trees Estimators

Leveraging on Theorem 12 and on previous works in FDA, we now tackle the problem of estimating merge trees of functions from noisy samples. In particular we assume the following standard functional model, which we call (M).

Definition 13 (Functional Statistical Model) *The functional model (M) is defined as follows. Consider a real random variable \mathcal{X} distributed with density p , supported on a compact interval. Consider a real random variable \mathcal{Y} such that $\mathcal{Y} \mid \mathcal{X} = x \sim f(x) + \varepsilon$, with ε being an independent noise variable with zero mean and finite variance. Moreover assume $p > \epsilon > 0$ on its support.*

In the following, we consider iid samples $\{(x_i, y_i)\}_{i=1}^n$ from (M); that is:

$$y_i = f(x_i) + \varepsilon_i, \quad (1)$$

for $i = 1, \dots, n$, from which we wish to estimate f .

We will estimate merge trees via regression estimators, which smooth the functions from which we obtain the trees; for this reason further assumptions may be needed depending on the choice of the functional smoother.

Remark 14 *As anticipated, the following theoretical developments have been obtained under assumptions (B) on the considered function. We believe that following the same path also for the multivariate scenario should lead to analogous results, but we leave this investigation to future works.*

Let $X = [a, b]$ be the support of p . In the following we need to work with Sobolev spaces $H^p([a, b])$ and functions of Bounded Variation $BV([a, b])$. We don't need to enter the details of weak derivatives and Sobolev norms, as we only work with continuously differentiable functions and with functions which are continuously differentiable up to a finite set of points. Thus, their respective weak derivatives are either the actual derivatives or the Lebesgue equivalence class identified by the pointwise derivative (when defined) in the second case (see Quarteroni and Valli (2008)). We always work on compact sets and bounded functions and so all our objects live in some Sobolev space coherently with their level of regularity. For BV functions, instead, we need to give some formal definition. For more details, refer to Rudin (1987).

Definition 15 *Define $\mathcal{P}([a, b])$ to be the set of all ordered finite sets of distinct points $x_1 = a < x_2 < \dots < x_m = b$.*

Given $f : [a, b] \rightarrow \mathbb{R}$, we define $V_{[a, b]}(f)$ as the total variation of f , given by:

$$V_{[a, b]}(f) = \sup_{p \in \mathcal{P}([a, b])} \sum_1^{\#p-1} |f(x_{i+1}) - f(x_i)|.$$

The functions with finite total variation on $[a, b]$ are collected in $BV([a, b])$.

It is well known that, for continuous functions admitting an absolutely integrable (weak) derivative we have:

$$V_{[a,b]}(f) = \int_{\mathbb{R}} |Df(x)| dx = \|Df\|_1,$$

where we indicate with $D^k f$ the k -th (weak) derivative of f . This is given by the Fundamental Theorem of calculus plus the following facts:

- for f monotone, $V_{[a,b]}(f) = |f(b) - f(a)|$;
- for any $c \in (a, b)$, $V_{[a,b]}(f) = V_{[a,c]}(f) + V_{[c,b]}(f)$.

More generally for a function f satisfying assumptions (B):

$$V_{[a,b]}(f) = \sum_1^{n-1} |f(x_{i+1}) - f(x_i)|,$$

with $\{x_1, \dots, x_n\}$ being the ordered sequence of the critical points of f .

The pivotal result of this section is the following.

Theorem 16 *Let $f : [a, b] \rightarrow \mathbb{R}$ be a function satisfying assumptions (B). If C_f is the number of local minima of f , then, for every $g \in \text{BV}([a, b])$ continuous with only isolated critical points, we have:*

$$d_E(T_f, T_g) \leq 8C_f \|f - g\|_{\infty} + |V_{[a,b]}(f) - V_{[a,b]}(g)|.$$

Remark 17 *Let $f, g \in \text{BV}([a, b])$ continuously differentiable functions. We know that $V_{[a,b]}(f - g) = \int_{[a,b]} |Df(x) - Dg(x)| dx$. Thus $|V_{[a,b]}(f) - V_{[a,b]}(g)| \leq V_{[a,b]}(f - g) \leq (b - a) \|Df - Dg\|_{\infty}$. As a consequence, $\|Df - Df_n\|_{\infty} \rightarrow 0$ implies $|V_{[a,b]}(f) - V_{[a,b]}(f_n)| \rightarrow 0$.*

Theorem 16 can be seen as some sort of “remainder” result, stating that if the oscillations of the difference between f and g decrease in amplitude fast enough, then we can control the distance between their merge trees (note that f must have a finite number of oscillations). Using Theorem 16 we can prove the following result, which states some conditions under which functional estimators can be used to build estimators of merge trees.

Proposition 18 *Given f continuously differentiable function on $X = [a, b]$ satisfying assumptions (B), let \hat{f}_n be a functional estimator of f obtained from $\{(x_i, y_i)\}_{i=1}^n$ sampled independently from (M) and such that, under suitable hypotheses, we have:*

1. $P(\|f - \hat{f}_n\|_{\infty} \leq \varepsilon) \geq 1 - h_n(\varepsilon)$;
2. $P(\|Df - D\hat{f}_n\|_{\infty} \leq \varepsilon) \geq 1 - g_n(\varepsilon)$;

for some positive functions h_n and g_n . Then:

$$P(d_E(T_f, T_{\hat{f}_n}) \leq 2\varepsilon) \geq 1 - h_n(C_1\varepsilon) - g_n(C_2\varepsilon) + h_n(C_1\varepsilon)g_n(C_2\varepsilon),$$

for some constants $C_1, C_2 > 0$.

4.3 Merge Trees Approximations

The one presented in the previous proposition, is an estimator based on being able to exactly compute the merge tree $T_{\hat{f}_n}$, for some consistent functional estimator \hat{f}_n . To do this, we need to determine the exact value and the nature of all the critical values of \hat{f}_n . Since, in practice, this may be very complicated, if not impossible, we now introduce an approximation scheme for merge trees of functions, which also leads to a consistent estimator that we can always compute.

Given $f : X \rightarrow \mathbb{R}$, consider $\{z_1, \dots, z_m\} \subset X$, with $z_i < z_{i+1}$, and obtain f_δ^{PL} as the piecewise affine function interpolating $\{(z_i, f(z_i))\}$, with $\delta = \max_{i=2, \dots, m} z_i - z_{i-1}$. The merge tree of f_δ^{PL} is an approximation of T_f whose convergence is established via the following result.

Proposition 19 *Consider a Lipschitz function $f : [a, b] \rightarrow \mathbb{R}$ with constant L , and a regular grid of points $\{z_1, \dots, z_m\} \subset [a, b]$. Let f_δ^{PL} be the piecewise affine function interpolating $\{(z_i, f(z_i))\}$, with $\delta = \max_{i=2, \dots, m} z_i - z_{i-1}$. Then:*

1. $\|f - f_\delta^{PL}\|_\infty \leq 2L\delta$;
2. $V_{[a,b]}(f - f_\delta^{PL}) \leq (b-a)^{1/2}A\delta \|D^2f\|_2$ for some constant $A > 0$ independent of f ;
3. $d_E(T_f, T_{f_\delta^{PL}}) \leq \Delta_f\delta$, with Δ_f being a constant depending only on f and $[a, b]$.

Theorem 19 states that piecewise affine interpolants can be used to approximate merge trees. The advantage of these functions is that their merge trees can be exactly computed, as their critical points are always a subset of the selected grid $\{z_1, \dots, z_m\} \subset [a, b]$, and their nature is easily assessed by looking at the ordering properties of the respective critical values.

Now we want to go full circle and exploit this fact to build computable estimators for merge trees. Given \hat{f}_n , a functional estimate of $f : [a, b] \rightarrow \mathbb{R}$, we select a uniform grid of points $\{z_1, \dots, z_m\} \subset [a, b]$ and obtain $\hat{f}_{n,m}^{PL}$ as the piecewise affine function interpolating $\{(z_i, \hat{f}_n(z_i))\}$. The merge tree of $\hat{f}_{n,m}^{PL}$ is our computational estimator. Note that, compared to Theorem 18, to prove the convergence of the estimator $T_{\hat{f}_{n,m}^{PL}}$, we need to increase assumptions on the regularity f and on the convergence of \hat{f}_n .

Proposition 20 *Given f two times continuously differentiable tame function on $[a, b]$, let \hat{f}_n be a functional estimator obtained from n points and such that, under suitable hypotheses, we have:*

1. $P(\|f - \hat{f}_n\|_\infty \leq \varepsilon) \geq 1 - h_n(\varepsilon)$;
2. $P(\|Df - D\hat{f}_n\|_\infty \leq \varepsilon) \geq 1 - g_n(\varepsilon)$;
3. $P(\|D^2f - D^2\hat{f}_n\|_\infty \leq \varepsilon) \geq 1 - q_n(\varepsilon)$

for some positive functions h_n , g_n and q_n . Let $\hat{f}_{n,m}^{PL}$ be the piecewise affine interpolant built from \hat{f}_n on a uniform grid of m points in $[a, b]$.

Then, there exists some constants C_1, \dots, C_4 , depending only on f , such that for every $m > C_4/\varepsilon$ we have:

$$P(d_E(T_f, T_{\hat{f}_{n,m}^{PL}}) < 4\varepsilon) \geq (1 - h_n(C_1\varepsilon))(1 - g_n(C_2\varepsilon))(1 - q_n(C_3\varepsilon/m)).$$

In the introduction we mentioned the problem of smoothing the data as one of the fundamental steps of a functional data analysis pipeline. This holds true also for the topological approach that we propose to analyse functions, and it does so on two levels:

1. the first level is that, in order to build a merge tree from a sample $\{(x_i, y_i)\}_{i=1}^n$, we need to choose a functional representation of our data. For instance the piecewise affine interpolant of $\{(x_i, y_i)\}_{i=1}^n$;
2. on a second level, the topological representation that we obtain from a functional representation of $\{(x_i, y_i)\}_{i=1}^n$ inherits the variability of the noisy observations depending on the roughness of the chosen functional representation. The rougher the functional representation, the noisier the tree i.e. the more there will be small artifacts (edges) increasing the size of the associated merge tree and distorting the metric d_E . Theorem 18 and Theorem 20 show that a careful smoothing of the functional representation is enough to obtain good estimates of merge trees, so one can proceed with the analysis taking advantage of the invariance properties described by Theorem 6. Lastly, note that the convergence of trees estimators is controlled by the convergence of the functional estimators. As a consequence, the choices of the hyperparameters of \hat{f}_n , like the bandwidth in case of kernel estimators, should be made according to classical criteria which have already been proposed to drive such decisions. We leave to future works the investigation of estimation methods working directly on merge trees, which can lead to estimators that can be employed also when merge trees are not used to represent functions, but also other kinds of data.

We now collect in a theorem some results proven in Schuster and Yakowitz (1979) as an example of a functional estimator which, under suitable conditions, satisfies Theorem 20.

Theorem 21 (adapted from Schuster and Yakowitz (1979)) *Consider the setting of model (M). Moreover, suppose:*

1. p is three times continuously differentiable;
2. q is the joint probability of $(\mathcal{X}, \mathcal{Y})$ and

$$w(x) = \int_{\mathbb{R}} yq(x, y)dy,$$

is three times continuously differentiable;

3. f is three times continuously differentiable;

Consider a univariate density K such that:

A) *we have:*

$$\int_{\mathbb{R}} |xK(x)| dx < \infty;$$

B) DK , D^2K and D^3K are continuous and of bounded variation on \mathbb{R} ;

C) $x\phi(x)$ and $x^2\phi(x)$ are absolutely integrable, with:

$$\phi(x) = \int_{\mathbb{R}} e^{iux} K(u)du,$$

being the characteristic function of K .

Then, given an iid sample $\{(x_i, y_i)\}_{i=1}^n$ from q and a sequence of bandwidths $a_n \rightarrow 0$, we can define:

$$\hat{f}_n(x) := \frac{\sum_{i=1}^n y_i K\left(\frac{x-x_i}{a_n}\right)/(na_n)}{\sum_{i=1}^n K\left(\frac{x-x_i}{a_n}\right)/(na_n)}$$

extended with 0 where the denominator is 0. Then, for any $\varepsilon > 0$ and n sufficiently large, we have:

$$P(\|D^j f - D^j \hat{f}_n\|_\infty < \varepsilon) > 1 - C/(na_n^{2j+2}\varepsilon^2).$$

Note that the Gaussian kernel satisfies the hypotheses of Theorem 21.

To conclude this section, we point out that the literature dealing with the topic of derivative estimation is very rich (Stone, 1985; Müller et al., 1987; Delecroix and Rosa, 1996; Chaudhuri and Marron, 1999; Zhou and Wolfe, 2000; Gijbels and Goderniaux, 2005; Fan, 2018; Liu and De Brabanter, 2020), encompassing also results on multivariate data (Akima, 1984; Lu, 1996), which can be used when extending these results to multivariate functions. For simplicity, in Theorem 21 and in our case study, we have chosen works (Schuster and Yakowitz, 1979; Müller, 1984; Mack and Müller, 1989) that enable us to use a very well-known estimator for nonparametric regression, namely the Nadaraya-Watson kernel estimator (Nadaraya, 1964), which was also used for other consistency results in the TDA setting (Fasy et al., 2014; Bobrowski et al., 2017). But the generality of Theorem 20 allows for other choices.

5. Case Study - Dataset

We now run a comparative analysis of the real world Aneurisk65 dataset. This dataset – and the clinical problem for which it was generated and studied – was first described in Sangalli et al. (2009b), but it has since become a benchmark for the assessment of FDA methods aimed at the supervised or unsupervised classification of misaligned functional data (see, for instance, the special issue of the Electronic Journal of Statistics dedicated to phase and amplitude variability - year 2014, volume 8). We then repeat the classification exercise illustrated in Sangalli et al. (2009b) with the double scope of comparing merge trees and persistent diagrams when used as representations of the Aneurisk65 misaligned functional data, and of evaluating the performance of these representations for classification purposes when compared with the results obtained with the more traditional FDA approach followed by Sangalli et al. (2009b).

The data of the Aneurisk65 dataset were generated by the AneuRisk Project, a multidisciplinary research aimed at investigating the role of vessel morphology, blood fluid dynamics, and biomechanical properties of the vascular wall, on the pathogenesis of cerebral aneurysms. The project gathered together researchers of different scientific fields, ranging from neurosurgery and neuroradiology to statistics, numerical analysis and bio-engineering. For a detailed description of the project scope and aims as well as the results it obtained see its web page (<https://statistics.mox.polimi.it/aneurisk>) and the list of publications cited therein.

Since the main aim of the project was to discover and study possible relationships between the morphology of the inner carotid artery (ICA) and the presence and location of cerebral aneurysms, a set of three-dimensional angiographic images was taken as part of an observational study involving 65 patients suspected of being affected by cerebral aneurysms and selected by the neuroradiologist of Ospedale Niguarda, Milano. These 3D images were then processed to produce 3D geometrical reconstructions of the inner carotid arteries for the 65 patients. In particular, these image reconstructions allowed to

extract, for the observed ICA of each patient, its centerline “raw” curve, defined as the curve connecting the centres of the maximal spheres inscribed in the vessel, along with the values of the radius of such spheres. A detailed description of the pipeline followed to identify the vessel geometries expressed by the AneuRisk65 functional data can be found in Sangalli et al. (2014).

Different difficulties arise when dealing with this data. First, as detailed in Sangalli et al. (2009a), to properly capture information affecting the local hemodynamics of the vessels, the curvature of the centerline must be obtained in a sensible way. Retrieving the salient features of the centerline and of its derivatives is a delicate operation, which is heavily affected by measurement errors and reconstruction errors, due to the complex pipeline involved. Consequently the “raw” curves appear to be very wiggly and it is not obvious how to produce reasonable smooth representations. At the same time the 3D volume captured by the angiography varies from patient to patient. This is due to many factors, such as: the position of the head with respect to the instrument, which in turns depends on the suspected position of the aneurysm, the disposition of the vessels inside the head of the patient, the size of the patient. As shown by Figure 7 in the appendix, one can recognize these differences even by visual inspection: for instance, in Figure 7a and Figure 7i we see a longer portion of the ICA than in Figure 7e. Therefore the reconstructed ICAs cannot be compared directly: we need methods that take into account that the centerlines are not embedded in \mathbb{R}^3 in the same way, and that we cannot expect potentially interesting features to appear in exactly the same spots along the centerline. This is the typical situation where one should resort to alignment.

Hence, this dataset is paradigmatic of the three-faceted representation problem highlighted in the introduction; data smoothing, embedding, and alignment present difficult challenges, which propelled a number of original works in FDA.

The AneuRisk65 data have been already partially processed; in particular centerlines have been smoothed following the free-knot regression spline procedure described in Sangalli et al. (2009a), and their curvatures were thus obtained after computing the first two derivatives of the smoothed curves. The data relative to the radius of the blood vessel, instead, although measured on a very fine grid of points along the centerline, is still in its raw format. Hence the AneuRisk65 data also allow us to compare the behaviour of tree representations on smoothed data and on raw data.

6. Case Study - Analysis

6.1 The pipeline for supervised classification

Patients represented in the AneuRisk65 dataset are organized in three groups: the Upper group (U) collects patients with an aneurysm in the Willis circle at or after the terminal bifurcation of the ICA, the Lower group (L) gathers patients with an aneurysm on the ICA before its terminal bifurcation, and finally the patients in the None group (N) do not have a cerebral aneurysm. Our main goal is supervised classification with the aim to develop a classifier able to discriminate membership to the group $L \cup N$ against membership to the group U based on the geometric features of the ICA. In the appendix, we complement this supervised analysis with a descriptive analysis of the merge trees, aggregated according to their group membership, and an unsupervised exercise which aims at clustering patients solely on the basis of the similarity of geometric features of their ICA, thus recovering a clear structure between the groups listed above and providing further support to the discriminating power of the geometric features of the ICA.

We develop a classification pipeline in close analogy with the one illustrated in Sangalli et al. (2009b) which, after smoothing and alignment, reduces the data dimensionality by means of Functional Principal Components Analysis (FPCA) applied to the curvature functions of the ICA centerlines and to the respective radius functions, and then fits a quadratic discriminant analysis (QDA) based on the first two FPCA scores of the curvature functions and of the radius functions respectively.

We replicate all the steps of their pipeline, except, of course, of the alignment step, which is not needed due to Theorem 6. We believe that this is a good way to proceed to compare the two approaches, as the considered pipelines differ only in the representations employed. More in details: we smooth the functions using the kernel smoothers presented in Müller (1984); Mack and Müller (1989), using the already smoothed curvature functions as “control group” for our bandwidth selection criterion, we extract merge tree representations of both radius and curvature functions and for each group we compute the matrices of pairwise distances using d_E . To merge the information contained in the two groups of functions, Sangalli et al. (2009b) joins the vectors containing the first two scores of the two group-wise FPCA. From the point of view of the pairwise distances between the patients, this amounts to considering the sums of the squared distances obtained respectively from the radius scores and curvature scores. More formally, if $c_{i,j}$ is the euclidean distance between the first two scores of the FPCA of curvature of patient i and patient j and $r_{i,j}$ is the analogous distance obtained from the radius FPCA, then the mixed distance $m_{i,j}$ obtained by joining the scores is equivalently given by:

$$m_{i,j}^2 = c_{i,j}^2 + r_{i,j}^2.$$

We do the same, blending the discriminatory information provided by curvature and radius, producing a new distance matrix according to the formula:

$$d_{\text{mixed}}^2 = d_{\text{curvature}}^2 + d_{\text{radius}}^2, \quad (2)$$

where $d_{\text{curvature}}$ and d_{radius} are respectively the pairwise distance matrices of the merge trees obtained from smoothed curvature and radius functions. For lack of references, we prove in Appendix I that d_{mixed} is a metric.

We then apply an euclidean non-linear embedding, namely Isomap (Balasubramanian and Schwartz, 2002), to d_{mixed} , in order to map the results in a finite dimensional Euclidean space of dimension m . Lastly, and following Sangalli et al. (2009b), we fit a QDA on such embedded points.

This pipeline requires the setting of two hyperparameters: the bandwidth of the kernel smoothers and the dimension m of the Euclidean embedding for MDS. While the bandwidth is chosen to improve the merge tree estimators convergence, see Section 6.2, the dimension m of the multidimensional scaling is selected by maximising the discriminatory power of QDA estimated by means of leave-one-out (L1out) cross-validation.

6.2 Kernel and Bandwidth Selection

In this section, we take a closer look at the smoothing carried out the curvature and radius function.

In order for the consistency results in Mack and Müller (1989) to be valid, we employ the kernel function:

$$K(x) = \frac{35}{32} \cdot (1 - 3x^2 + 3x^4 - x^6)$$

supported on $[-1, 1]$. As proven in Müller (1984), $K(x)$ fits into the desired framework, belonging to the therein defined space of functions $\mathcal{M}_{0,2}$. The functional estimator, then,

is:

$$\hat{f}_n^h(x) := \frac{\sum_{i=1}^n y_i K\left(\frac{x-x_i}{h}\right)}{\sum_{i=1}^n K\left(\frac{x-x_i}{h}\right)},$$

with n being the cardinality of the considered sample $\{(x_i, y_i)\}_{i=1}^n$, which we assume iid from model (M), and $h > 0$ being a fixed bandwidth we need to select.

According to Theorem 20 we want to choose h to improve the convergence of the merge estimators which rely on the convergence of \hat{f}_n^h , $D\hat{f}_n^h$, and $D^2\hat{f}_n^h$.

Thus, for the chosen kernel, we can use Equation (3.6) in Mack and Müller (1989), with $k = 4$ and $\nu = 2$ obtaining the following optimal local bandwidth for derivatives convergence:

$$h_x = \left(\frac{4! \mathbb{E}(\mathcal{Y}^2 \mid \mathcal{X} = x) \int_{-1}^1 D^2 K(t)^2 dt}{D^4 f(x)^2 \left(\int_{-1}^1 D^2 K(t) t^4 dt \right)} \right)^{1/9} \cdot n^{-1/9}. \quad (3)$$

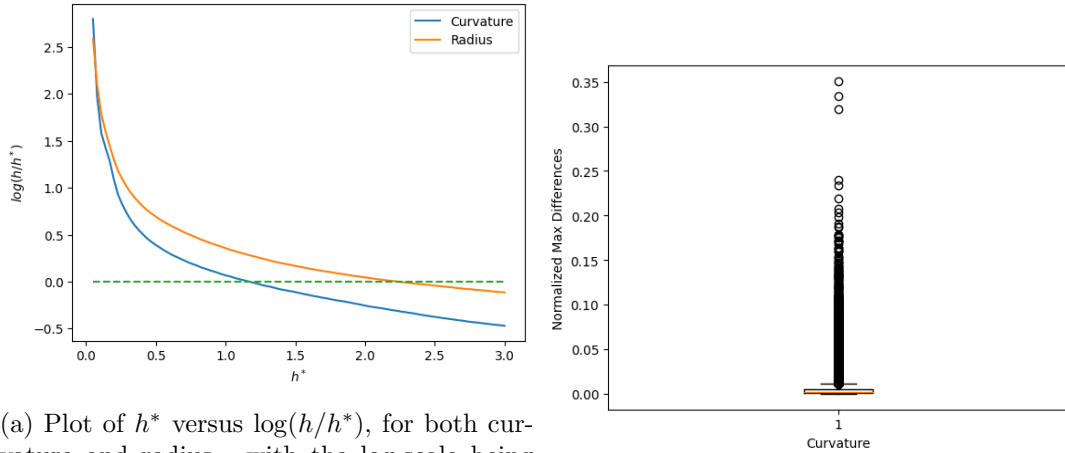
The use of this local bandwidth requires the further estimation of two quantities: 1) $\mathbb{E}(\mathcal{Y}^2 \mid \mathcal{X} = x)$ 2) $D^4 f(x)^2$. Following Mack and Müller (1989), we estimate $\mathbb{E}(\mathcal{Y}^2 \mid \mathcal{X} = x)$ with another kernel regression, whose bandwidth we select via Generalized Cross Validation Score (Kauermann and Opsomer, 2004), which is known to be prone to overfitting, and $D^4 f(x)^2$ with $D^4 \hat{f}_n^{h^*}(x)^2$. In particular, this estimate requires providing another bandwidth h^* . While Mack and Müller (1989) doesn't provide further insights on this choice, we used this additional hyperparameter to improve the estimate of h_x .

The upcoming procedure was used both for curvature and radius data (separately). For every $h^* \in (0, 3]$ we:

1. consider the data of the k -th patient $\{(x_i, y_i)\}_{i=1}^n$ and obtain the local bandwidth h_{x_j} plugging in $D^4 \hat{f}_n^{h^*}(x_j)^2$ in Equation (3);
2. obtain \hat{h}_k^* averaging h_{x_j} over all the points x_j ;
3. obtain h averaging h_k^* over all patients;
4. compare h with h^* : they are bandwidths plugged in the same kernel functions, used on the same data. If $h^* \gg h$, then our initial "guess" h^* was severely oversmoothing the data, and Equation (3) corrects this choice and shrinks the bandwidth locally, giving a much smaller \hat{h}^* . Viceversa, if $h^* \ll h$, h^* was undersmoothing the data, and Equation (3) returns a more generous bandwidth. This is also shown in Figure 5, which clearly shows that as h^* grows, the ratio h/h^* diminishes, and viceversa.

As a consequence of what we just stated, we chose h so that $h/\hat{h}^* = 1$. For the radius data we obtained a value $h_r = 2.25$ and for curvature $h_c = 1.15$. Which is coherent with the radius functions being much more wiggly, compared to the curvature ones which have already undergone a smoothing step.

To further support our choices we focus on what happens to the curvature data. In particular we measure the pointwise differences between the function before and after the additional smoothing we propose, normalizing by the range of the "raw" data. We report the boxplot of these pointwise differences in Figure 5, showing that the additional smoothing we do is in fact consistent with the work previously done in Sangalli et al. (2009a).



(a) Plot of h^* versus $\log(h/h^*)$, for both curvature and radius - with the log-scale being used to emphasize the behaviour of the curves for higher values of h^* . The green dotted line represents the threshold after which the bandwidth h^* oversmooths the data. The values of h_c and h_r are chosen at the intersection of the dotted line with the respective curves. The curves clearly show that the curvature data is much smoother, compared to radius, as the ratio h/h^* decreases much faster.

(b) We compare the pointwise differences in the curvature data before and after our supplementary smoothing. Looking at the boxplot of these differences, normalized by the range of the given function we see that our additional smoothing is coherent with the one previously done by Sangalli et al. (2009a).

Figure 5: Plots to support the bandwidth choice described in Section 6.2.

6.3 Classification Results

We compare our classification results with those illustrated in Sangalli et al. (2009b). The goal is the same: separating the class U from the classes L and N. Table 1, in the appendix, reports the detailed prediction errors obtained after L1out cross-validation.

To further prove the relevance of Theorem 6, the same pipeline is followed also choosing persistence diagrams instead of merge tree to represent the smoothed curvature and radius functions. Moreover, to highlight the differences between merge trees and PDs (on top of the simulations developed in the appendix), we explore the results obtained when feeding to the respective pipelines just the curvature or the radius data.

From the results we obtained (see the first two rows in Table 1), we observe that PDs do a better job in extracting useful information from radius, when examined separately. This could be due to a situation not dissimilar from that illustrated in the example of Appendix C.1: the discriminant information contained in the curvature and radius functions lies more in the number and amplitude of oscillations than in their ordering. However, when curvature and radius of the ICA are jointly considered as descriptors and the distance of Equation (2) is used, we obtain a better classifier for merge trees while for PDs accuracy decreases.

This situation highlights that merge trees and persistence diagrams capture different but highly correlated pieces of information about the current functional data set; note, however, that PDs suggest that most of the information they capture is due to the radius function, while merge trees show some informative interactions between curvature and radius.

The number of patients misclassified by the best classifier based on merge trees is slightly smaller than that of the best classifier based on PDs - see Table 1, but, despite

the profound differences between the two topological summaries (see Section 2.7, Appendix C.1, Appendix C.2 and Appendix C.3) the two methods are retrieving similar discriminant information related to the classification task: comparing the two analysis we found that 7 patients were misclassified by both methods. For comparison, the prediction errors of the best classifiers based on merge trees and on PDs are reported in the third column of Table 1 in the appendix, while in the last row the reader can find the prediction errors of the classifier described in Sangalli et al. (2009b).

7. Discussion

We believe that methods from TDA can be fruitfully added to the toolbox of functional data analysis, especially when non trivial smoothing and alignment are required for data representation. In this paper we focused on two topological representations of functions: persistence diagrams, which, being the most classical tool in TDA, are regarded as a benchmark, and merge trees, which are rarely used in real data analysis applications. The framework for merge trees is the very recent metric structure defined in Pegoraro (2024b), for which we also developed theoretical results specific for the application to functional data.

To support our narrative, we used as paradigmatic real world application the classification analysis of the AneuRisk65 functional data set. This data set poses all the desired challenges: careful smoothing procedures and alignment techniques must be employed to obtain meaningful results. Reanalyzing the seminal case study described in Sangalli et al. (2009b), we showed the advantages of having a representation of functional data which is invariant with respect to homeomorphic transformations of the abscissa, lightening the burden of careful alignment. Following a classification approach based on QDA applied to properly reduced representations of the data, as in Sangalli et al. (2009b), we obtain robust results with comparable, if not better, accuracy in terms of L1out prediction error, and we confirm some facts about the variability of the data in the groups of patients characterized by the different location of the cerebral aneurysm, consistently with the findings of previous works.

The effectiveness of the simple pipeline proposed in the case study does motivate further research in order to deal with more complicated scenarios including multivariate functional data in which a vector of functions defined on the same domain could be summarized via a topological representation. Similarly, statistical tools to better interpret population of trees should be studied and developed. The existence of Frechét means in the space of merge trees (Pegoraro, 2024a) may lead to extensions of the frameworks found in Bhattacharjee and Müller (2023); Dubey and Müller (2022), which however would need to replace the uniqueness of geodesics and Frechét means assumptions either with some locality assumption, that is, fixing some particular open sets, or with some more general idea to ensure well-posedness of definitions and the needed statistical theory. Note that linearizing the space of trees via classical graph embeddings, like the laplacian one (Zhou and Müller, 2022), cannot be done it would lack the desired stability properties. Still, developing such tools would open up the door for more refined statistical procedures like testing or uncertainty quantification, which are very hard to deal with in general metric spaces. On top of that, optimizing the numeric and computational aspects of the tree-based tools that we introduced would surely make them more viable in applications.

To be sure, we want to stress that careful smoothing is still mandatory for precise estimation of merge trees and when precise differential information about the data is needed. Moreover, not all FDA applications are adapted to the representations offered

by merge trees or persistent diagrams. Indeed, the information collected by merge trees is contained in the ordering and in the amplitude of the extremal points of a function, and not on their exact abscissa. Hence, if the abscissa carries valuable information for the analysis – for instance, a wavelength, or a precise landmark point in space or time – the TDA approach followed in this work for data representation is not indicated, precisely because of its invariance property with respect to homeomorphic transformations of the abscissa. But this criticism also applies to many alignment procedures proposed in the literature. Similarly, in Appendix C.2, we point out that there are functions which have equivalent representations in terms of merge trees although the order on the abscissa of their critical points is different, in spite of the fact that merge trees are much less sensitive to such issue when compared to persistence diagrams (see also Kanari et al. (2020)). If the order of critical points of the function is of importance for the analysis, then surely persistence diagrams, but possibly also merge trees, should be avoided.

More generally, we point out that whenever the datum designating a statistical unit is only a representative of an equivalence class, the analyst must be sure that the variability differentiating the members of the same class is ancillary with respect to the statistical analysis performed on the statistical units. This consideration always applies in FDA, whenever data are aligned according to transformations belonging to a group. Merge trees offer a representation of functional data in terms of equivalence classes whose members are invariant with respect to homeomorphic transformations of the abscissa. Persistence diagrams partition the space of functional data in even coarser equivalence classes, although they could be enough for the analysis, as we saw in the case study illustrated in Section 5. Occam’s razor should guide the analyst’s final choice.

8. Acknowledgements

We thank Steve Marron who initiated us to algebraic topology for the statistical analysis of functional data during seminal discussions while one of us (PS) was visiting him at UNC. We thank the AneuRisk Project for providing the data analyzed in the case study. We also deeply thank the editor and the reviewers for their very helpful and constructive comments which contributed to a significant improvement of the original manuscript.

Appendix A. Additional Figures and Tables

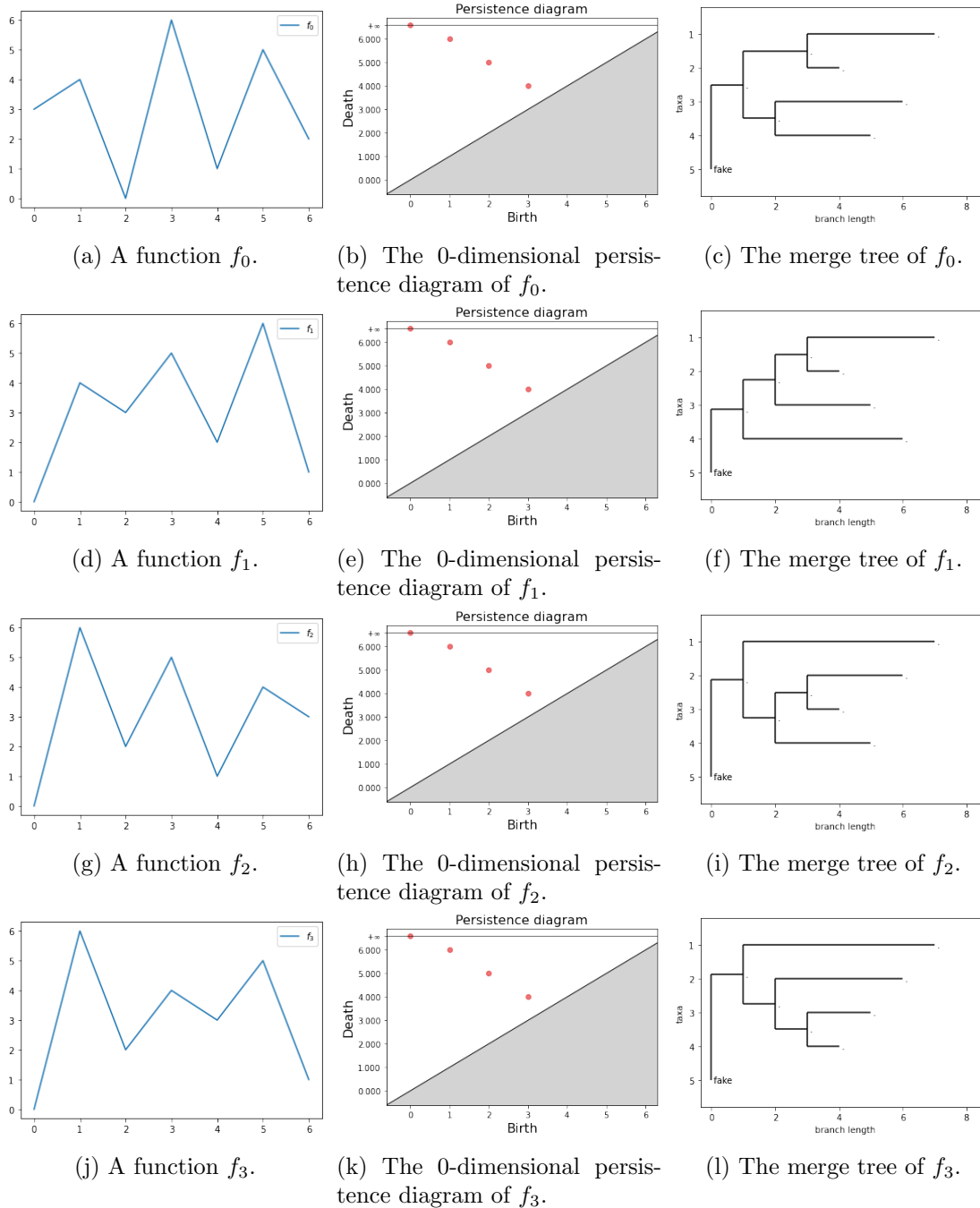
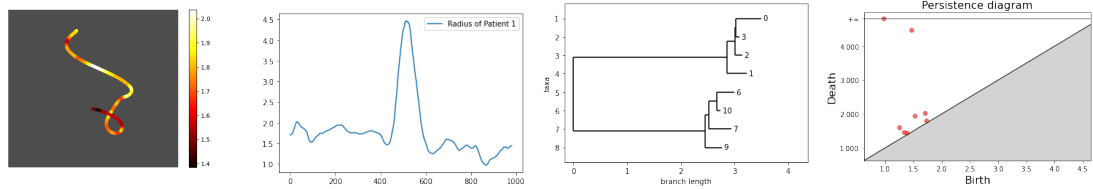
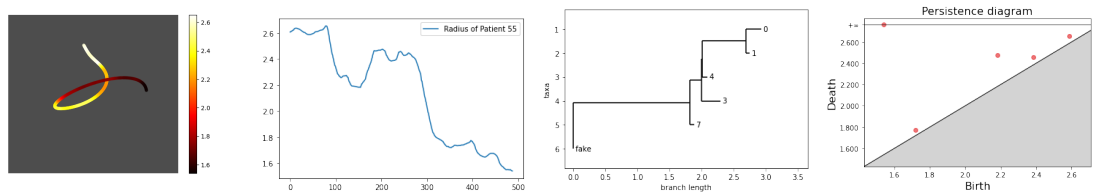


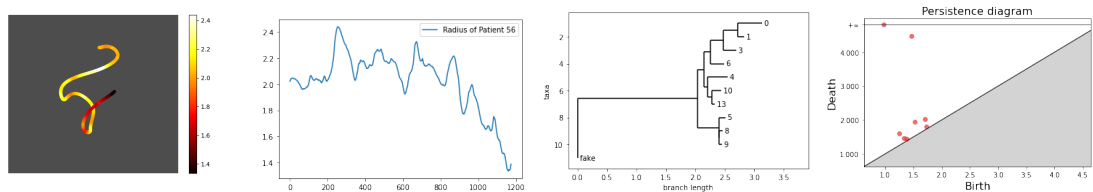
Figure 6: A visual example highlighting differences between PDs and merge trees. We consider four functions all associated to the same PD but to different merge trees. Functions are displayed in the first column and on each row we have on the centre the associated PD and on the right the merge tree. All merge trees are truncated at height 7 - see Section 2.6.



(a) ICA patient 1 (L). (b) Radius along the ICA of patient 1 (L). (c) Merge tree associated to the radius function of patient 1 (L). (d) Persistence diagram associated to the radius function of patient 1 (L).



(e) ICA patient 55 (U). (f) Radius along the ICA of patient 55 (U). (g) Merge tree associated to the radius function of patient 55 (U). (h) Persistence diagram associated to the radius function of patient 55 (U).



(i) ICA patient 56 (U). (j) Radius along the ICA of patient 56 (U). (k) Merge tree associated to the radius function of patient 56 (U). (l) Persistence diagram associated to the radius function of patient 56 (U).

Figure 7: Three patients in the AneuRisk65 dataset; on the first column of the left, the ICAs of the patients are coloured according to the radius value, on the second column there are the radius functions, on the third column their associated merge trees and on the rightmost column the persistence diagrams. Patient 1 belongs to the Lower group (L), the other two patients to the Upper group (U). Note that the merge trees have been truncated with K equal to the maximum of Figure 7b.

		Merge Trees					
		Curvature		Radius		Mixed	
		$\{U\}$	$\{L, N\}$	$\{U\}$	$\{L, N\}$	$\{U\}$	$\{L, N\}$
True	$\{U\}$	22	10	21	11	25	7
	$\{L, N\}$	3	30	4	29	3	30
		$n = 4$		$n = 7$		$n = 7$	
		Persistence Diagrams					
		Curvature		Radius		Mixed	
		$\{U\}$	$\{L, N\}$	$\{U\}$	$\{L, N\}$	$\{U\}$	$\{L, N\}$
True	$\{U\}$	23	9	28	4	27	5
	$\{L, N\}$	4	29	6	27	L	27
		$n = 9$		$n = 7$		$n = 7$	
		Benchmark					
		Curvature		Radius		Mixed	
		$\{U\}$	$\{L, N\}$	$\{U\}$	$\{L, N\}$	$\{U\}$	$\{L, N\}$
True	$\{U\}$	26	6	26	6		
	$\{L, N\}$	6	27	6	27		

Table 1: Confusion matrices (L1out) for the different classification pipelines presented in Section 5. Below each confusion matrix, the value of the dimension n for Isomap corresponding to the tested classifier is reported. The first row refers to the classifiers receiving as input merge tree representations, the second row PDs. The last row reports the benchmark L1out confusion matrix for the classifier illustrated in Sangalli et al. (2009b).

Appendix B. Topological Remark

Let us now see how we can represent a real valued function $f : X \rightarrow \mathbb{R}$ by means of a merge tree, under conditions (A0) - introducing also the formal definition of *tameness*. To do so, we need to make some key assumptions, known in the literature to be apt to produce *constructible* objects (De Silva et al., 2016; Patel, 2018; Curry et al., 2022).

Assumption 2 (Tameness) *Given a family of topological spaces $\{X_t\}_{t \in \mathbb{R}}$ with $X_t \subset X_{t'}$, $t \leq t'$, we assume the existence of a finite collection of real numbers $\{t_1 < t_2 < \dots < t_n\}$, called *critical set*, such that, given $t < t'$, if $t, t' \in (t_i, t_{i+1})$ or $t, t' > t_n$, then $\pi_0(i_t^{t'})$ is bijective. The values t_i are called *critical values*. As in Pegoraro (2024b) we always consider a minimal set of critical values, that is, the smallest possible set of critical values. With this condition, for any critical value t_i there is some constant $C > 0$ such that for all $\varepsilon \in (0, C)$, $\pi_0(i_{t_i - \varepsilon}^{t_i + \varepsilon})$ is not bijective. Moreover, we assume that for every $t \in \mathbb{R}$, $\pi_0(X_t)$ is finite. A function $f : X \rightarrow \mathbb{R}$ such that its sublevel set filtration $\{X_t\}_{t \in \mathbb{R}}$ satisfies the above set of hypotheses is called *tame* (Chazal et al., 2016). Lastly, we also assume that X is path connected.*

Together with the tameness of f and the path-connectedness of X , - which constitute assumptions (A0) - we make an extra and simplifying *regularity* assumption - not needed, for the general construction of a merge tree - which implies a strong property of the critical values of the sublevel set filtration $\{X_t\}_{t \in \mathbb{R}}$ of f . This assumption can in fact be weakened,

at the cost of some non trivial topological details (for more details see also Pegoraro (2024b)).

Let t_j be a critical value of the sublevel set filtration $\{X_t\}_{t \in \mathbb{R}}$ of f . Let $\varepsilon > 0$ be such that $t_j - \varepsilon > t_{j-1}$ and $t_j + \varepsilon < t_{j+1}$. The properties of π_0 imply that $\pi_0(i_{t_j - \varepsilon}^{t_j + \varepsilon}) = \pi_0(i_{t_j - \varepsilon}^{t_j}) \circ \pi_0(i_{t_j}^{t_j + \varepsilon})$. Due to the minimality condition stated in Assumption 2 we know that $\pi_0(i_{t_j - \varepsilon}^{t_j + \varepsilon})$ is not bijective.

Assumption 3 (Regularity) *We assume that the sublevel set filtration $\{X_t\}_{t \in \mathbb{R}}$ of f is regular: that is, for every critical value t_j of $\{X_t\}_{t \in \mathbb{R}}$, there is a $C > 0$ such that, for all $\varepsilon \in (0, C)$, the map $\pi_0(i_{t_j}^{t_j + \varepsilon})$ is bijective. When $\pi_0(i_{t_j}^{t_j + \varepsilon})$ is bijective, we say that the topological changes happen at the critical value t_j , as opposed to across t_j . Hence we are assuming that all the topological changes of $\{X_t\}$ happen at the critical values.*

From the topological point of view, what lies behind the requirement that the topological changes happen at critical values is the following. Let $U_{t_j} \in \pi_0(X_{t_j})$ and $U_t = \pi_0(i_{t_j}^t)(U_{t_j})$ for $t \in (t_j, t_{j+1})$. By construction, $U_{t_j} \subset U = \bigcap_{t \in (t_j, t_{j+1})} U_t$ and $f(p) = t_j$ for all $p \in U$. Which means $U \subset X_{t_j}$. If U is path connected then $U_{t_j} = U$ and we can't have another path connected component $U'_{t_j} \in \pi_0(X_{t_j})$ such that $U'_{t_j} \subset U$.

All of this implies that, for $t \in (t_j, t_{j+1})$, $\pi_0(i_{t_j}^t)^{-1}(U_t) = \{U_{t_j}\}$ - i.e. $\pi_0(i_{t_j}^t)$ is injective at U_{t_j} and $U_t \in \pi_0(i_{t_j}^t)(\pi_0(X_{t_j}))$. So, if for every path connected component $U_{t_j} \in \pi_0(X_{t_j})$ the set $U = \bigcap_{t \in (t_j, t_{j+1})} \pi_0(i_{t_j}^t)(U_{t_j})$ is non empty and path connected, then $\pi_0(i_{t_j}^t)$ is bijective. However, in general, U need not be non empty and path connected!

Two notable cases where the topological changes happen at critical values are that of a continuous function f defined on a connected compact subset of \mathbb{R} and that of an f defined on a finite graph.

Indeed, let $f : X \rightarrow \mathbb{R}$ be continuous and $X \subset \mathbb{R}$ be a compact interval. Then, for all $t \in \mathbb{R}$, X_t is closed, since f is continuous, and its path connected components are compact intervals of the form $[a, b]$. Each path connected component U_{t_j} is thus a convex set and any intersection of the form $U = \bigcap_{t \in (t_j, t_{j+1})} \pi_0(i_{t_j}^t)(U_{t_j})$ is non-empty and convex; that is, U is non empty and path connected. Thus, for continuous functions $f : X \rightarrow \mathbb{R}$, with $X \subset \mathbb{R}$ being a compact interval, the topological changes always happen at critical values.

Consider now the discrete setting of a finite graph $X = (V, E)$, with vertices V and edges E , such that the sublevel set filtration is well defined (i.e. for any edge $e_{ij} = (x_i, x_j) \in E$ connecting two vertices x_i and x_j , we have $f(e) \geq \max\{f(x_i), f(x_j)\}$). Let $t_1 < t_2 < \dots < t_n$ be the image of f . Then, $X_t = X_{t_j}$ for all $t \in [t_j, t_{j+1})$. This implies that all topological changes happen at critical values.

As a consequence, all the functions considered in the present work, those illustrated in the examples or those pertaining to the case study described in Section 5, do satisfy our Assumption 3, and the same is true for all numerical implementations.

However, not all scenarios satisfy the regularity condition, as we can see in the upcoming examples.

Example I Consider the following sequences of topological spaces $\{A_t\}_{t \in [0, \infty)}$ and $\{B_t\}_{t \in [0, \infty)}$. For $t > 0$, let $A_t = (-t, t) \cup (1 - t, 1 + t)$ and $B_t = [-t, t] \cup [1 - t, 1 + t]$. Moreover, let $A_0 = B_0 = \{0, 1\}$. $\{A_t\}$ and $\{B_t\}$ share the same set of critical values, namely $\{0, 1/2\}$ and they only differ by the number of path connected components at the critical value $1/2$: $\#A_{1/2} = 2$, while $\#B_{1/2} = 1$. In $\{A_t\}$ changes happen across the critical values - $\pi_0(A_{1/3}) \cong \pi_0(A_{1/2})$ and $\pi_0(A_{1/2}) \not\cong \pi_0(A_1)$, while in $\{B_t\}$ changes happen at the critical values - $\pi_0(B_{1/3}) \not\cong \pi_0(B_{1/2})$ and $B_{1/2} \cong B_1$.

Example II Consider the following sequence of topological spaces $\{A_t\}_{t \in [0, \infty)}$. For $t > 0$, let $A_t = \{(-\infty, +\infty) \times [-1/t, 1/t]\} - \{(0, 0)\}$ and $A_0 = \{(-\infty, 0) \cup (0, +\infty)\} \times \{0\}$. Then $\bigcap_{t > 0} A_t = A_0$: however A_0 has two path connected components while, for $t > 0$, the set A_t is path connected.

Example III Let $\gamma : (0, 1] \rightarrow \mathbb{R}^2$ defined by $\gamma(t) = (t, \sin(1/t))$. Let T be the closure in the plane of the set $S = \{(t, \gamma(t)) \in \mathbb{R}^2 : t \in (0, 1]\}$, which is given by $T = S \cup \{0\} \times [-1, 1]$. The set S is usually referred to as the topologist's sine curve and the set T as the closed topologist's sine curve. Let S_n be:

$$S_n = \{(t, s) \mid t \in [1/n, 1] \text{ and } s \in [\sin(1/t) - 1/n, \sin(1/t) + 1/n]\}$$

That is, S_n is an $1/n$ -thickening along the y -axis (second component of \mathbb{R}^2), of the graph of γ restricted on the interval $[1/n, 1]$. Thus, if we add to S_n the rectangle $R_n = [-1/n, 1/n] \times [-1 - 1/n, 1 + 1/n]$ we obtain a set $T_n = S_n \cup R_n$ such that:

- $T = \bigcap_{n \in \mathbb{N}} T_n$
- T_n is compact and path connected. It is in fact homeomorphic to $R_n \cup [1/n, 1] \times [-1/n, 1/n]$ and thus homeomorphic to a closed disk in the plane.

As $n \rightarrow \infty$ we obtain a family of compact "disks" whose intersection is T which is not path connected.

Example IV Lastly $A_t = [1/t, +\infty) = f^{-1}((-\infty, t])$ with $f : \mathbb{R}_{>0} \rightarrow \mathbb{R}$ being $f(x) = 1/x$. Clearly A_t is closed and path connected, but $\bigcap_{t > 0} A_t$ is empty.

In all the examples above we see different situations in which at some critical point t we have a very "unstable" topological scenario, which changes at $t + \varepsilon$ for any small $\varepsilon > 0$:

- in Example I the balls centered in 0 and 1 contained in A_t touch right after $t = 1/2$; in fact their closures (giving $B_{1/2}$) at $t = 1/2$ would intersect;
- in Example II the horizontal stripe given by A_t suddenly disconnects at $t = 0$ because it is no more thick enough to get around the hole in $(0, 0)$;
- we find a very similar situation also in Example III, where every thickening of T would allow us to bridge between its two path connected components;
- lastly, in Example IV, we have a path connected component being born with a minimum "lying" at $+\infty$, thus producing an empty level set at $t = 0$.

The general point of view which we assume to build merge trees from irregular tame filtrations, which is formalized in Pegoraro (2024b), is that we deem to be negligible the topological differences between $\{A_t\}$ and $\{B_t\}$ in Example I, as those two filtrations have the same path connected components but for one point, $t = 1/2$, which we may look at as a measure zero subset of the parameter space indexing the filtration (i.e. \mathbb{R}). Thus, for all these examples, and, in fact, for all the *tame* filtrations of path connected topological spaces, we propose to build the associated merge tree as if all topological changes happen at critical points: if we have a critical point t_j such that $\pi_0(i_{t_j}^{t_j+\varepsilon})$ is not bijective, instead of looking at the merging information contained in $\pi_0(i_{t_{j-1}}^{t_j})$ - as we do in Section 2.4 - one should look at $\pi_0(i_{t_{j-1}}^{t_j+\varepsilon})$, but still recording the topological changes with a vertex at height t_j . In this way, for instance, the merge trees associated to $\{A_t\}$ and $\{B_t\}$ in Example I would be the same, in Example II we would have a single leaf at height 0 - despite A_0

having two path connected components, the same for Example III (upon replacing n with $1/\varepsilon$), and, lastly, Example IV would feature a leaf at height 0 despite A_0 being empty.

Having sorted out all these technicalities, we can finally build a merge tree from a tame and regular filtration of topological spaces $\{X_t\}_{t \in \mathbb{R}}$.

We build the merge tree (T, h_T) from $\{\pi_0(X_t)\}_{t \in \mathbb{R}}$ with the following rules, in a recursive fashion, starting from an empty set of vertices V_T and an empty set of edges E_T . We simultaneously add points and edges to T and define h_T on the newly added vertices. Let $\{t_i\}_{i=1}^n$ be the critical set of $\pi_0(X_\cdot)$ and let $\pi_0(X_t) := a_t := \{a_1^t, \dots, a_{n_t}^t\}$. Call $\psi_t^{t'} := \pi_0(X_{t \leq t'})$.

Considering in increasing order the critical values:

- for the critical value t_1 add to V_T a leaf $a_{t_1}^k$, with height t_1 , for every element $a_{t_1}^k \in a_{t_1}$;
- for t_i with $i > 1$, for every $a_{t_i}^k \in a_{t_i}$ such that $a_{t_i}^k \notin \text{Im}(\psi_{t_{i-1}}^{t_i})$, add to V_T a leaf $a_{t_i}^k$ with height t_i ;
- for t_i with $i > 1$, if $a_{t_i}^k = \psi_{t_{i-1}}^{t_i}(a_{t_{i-1}}^s) = \psi_{t_{i-1}}^{t_i}(a_{t_{i-1}}^r)$, with $a_{t_{i-1}}^s$ and $a_{t_{i-1}}^r$ distinct basis elements in $a_{t_{i-1}}$, add a vertex $a_{t_i}^k$ with height t_i , and add edges so that the previously added vertices

$$v = \arg \max\{h_T(v') \mid v' \in V_T \text{ s.t. } \psi_{t_{i-1}}^{t_i}(v') = a_{t_i}^k\}$$

and

$$w = \arg \max\{h_T(w') \mid w' \in V_T \text{ s.t. } \psi_{t_{i-1}}^{t_i}(w') = a_{t_i}^k\}$$

connect with the newly added vertex $a_{t_i}^k$.

The last merging happens at height t_n and, by construction, at height t_n there is only one point, which is the root of the tree structure.

These rules define a tree structure with a monotone increasing height function h_T . In fact, edges are induced by maps $\psi_t^{t'}$ with $t < t'$ and thus we can have no cycles and the function h_T must be increasing. Moreover, we have $\psi_t^{t_n}(a_i^t) = a_1^{t_n}$ for every i and $t < t_n$ and thus the graph is path connected.

Appendix C. Examples

C.1 Example I

In these sections, we present some examples which are intended to put to work the pruning operator and further show the differences between persistence diagrams and merge trees, already highlighted in Section 2.7 of the manuscript.

We devote Appendix C.1 to giving further intuition on the topic of functions being distinguished by merge trees but being represented by the same persistence diagram. Appendix C.2 and Appendix C.3 instead give a more qualitative idea of what kind of variability between functions is better captured by PDs and merge trees with, respectively, the 1-Wasserstein metric and the edit distance.

In this first example we produce a set of functions which are all described by the same persistence diagram but are distinguished by merge trees.

We want to exploit that, for continuous functions in one real variable, the merging structure of the path connected components (and so the tree structure T) is characterized by how local minima distribute on different sides of local maxima. We create a very simple toy situation: we define functions which have all a very high peak and a number of smaller

peaks of the same height, but with a different disposition of these smaller peaks with respect to the highest one.

For $i = 0, \dots, 9$, let $g_i : [0, 11] \rightarrow \mathbb{R}$ be such that $g_i \equiv 0$ on $[0, 11] - [i + 1/3, i + 2/3]$ while, on $[i + 1/3, i + 2/3]$, g_i is the linear interpolation of $(i + 1/3, 0)$, $(i + 1/2, 1)$ and $(i + 2/3, 0)$. Then, for $i = 0, \dots, 9$, define G_i as $G_i \equiv 0$ on $[0, 11] - [i + 2/3, i + 1]$ while, on $[i + 2/3, i]$, G_i is the linear interpolation of $(i + 2/3, 0)$, $(i + 3/4, 5)$ and $(i + 1, 0)$.

Then, for $i = 0, \dots, 9$, f_i is obtained as follows:

$$f_i = G_i + \sum_{j=0}^{10} g_j.$$

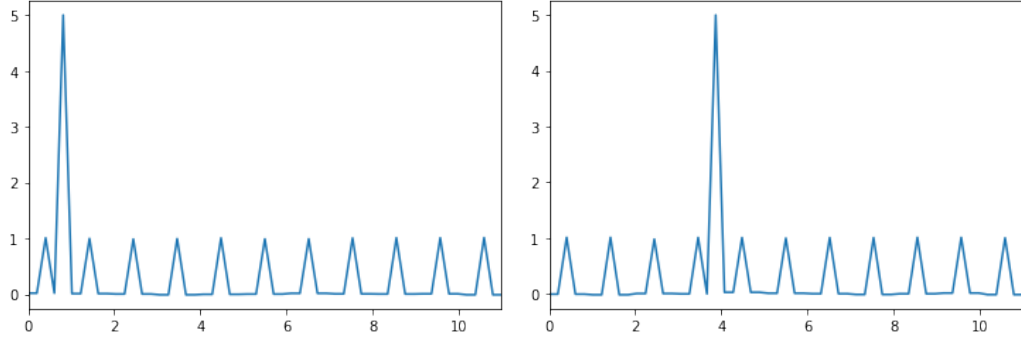
The functions f_0 and f_3 are displayed in Figure 8a. Note that the first and the last peak of every function, by construction, are always small peaks. The key point is that for every path connected component we are not changing any of the corresponding critical values and thus the associated persistence diagram is always the same (see Figure 8c).

The shortest edit path between two merge trees T_{f_i} and $T_{f_{i+1}}$ is given by the deletion of one leaf in each tree to make the disposition of leaves coincide between the two trees. The more the peak disposition is different between the two trees, the more one needs to delete leaves in both trees to find a shortest path between them. Thus, if we fix the first line of the matrix in Figure 8d, we see that going left-to-right the distance at first gradually increases. It is also evident that, from a certain point on, the distance decreases to the point of reaching almost zero. This is because the first function (the one in which the highest peak is the second peak) and the last function (the one in which the highest peak is the second-to-last peak) can be obtained one from the other via a y -axis symmetry and a translation $-x \mapsto -x$ (reflection on the y -axis) and $x \mapsto v + x$, with $v \in \mathbb{R}$ fixed (translation), these transformations being homeomorphisms of the abscissa. Similarly, the second function is equal, up to homeomorphic alignment, to the third-to-last one, etc.. Thus by Theorem 6 the merge trees are the same. To sum up the situation depicted in the first row of Figure 8d, first we get (left-to-right) farther away from the first merge tree, and then we return closer to it. This intuition is confirmed by looking at the MDS embedding in \mathbb{R}^2 of the pairwise distance matrix (see Figure 8e - note that the shades of gray reflect, from white to black, the ordering of the merge trees). The discrepancies between the couple of points which should be identified are caused by numerical errors.

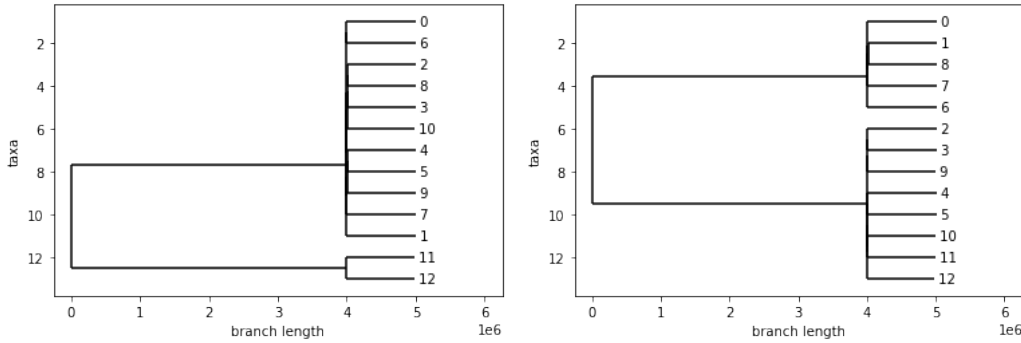
C.2 Example II

In this second example we want to produce a situation in which the variability between functional data is better captured by PDs than by merge trees. Accordingly, we generate two clusters of functional data such that membership of a function to one cluster or the other should depend on the amplitude of its oscillations and not on the merging structure of its path connected components. We then look at the matrices of pairwise distances between functions, comparing merge tree and persistence diagram representations in terms of their goodness in identifying the clustering structure.

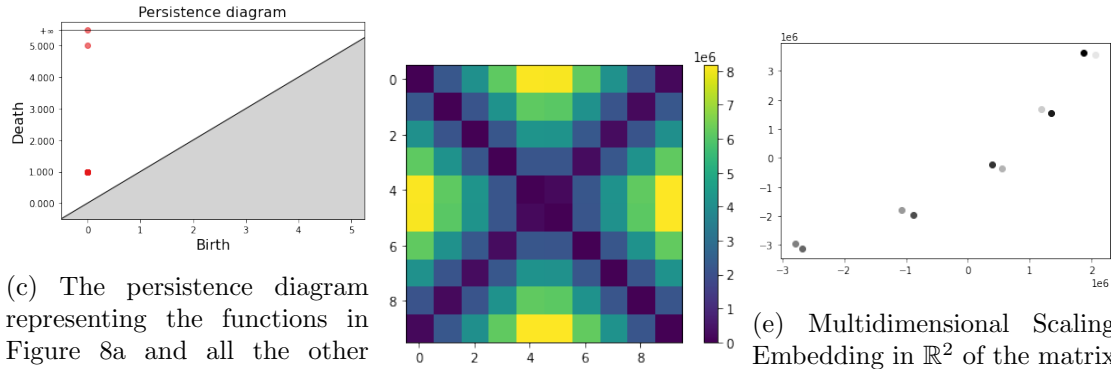
To generate each cluster of functions, we draw, for each cluster, an independent sample of 16 critical points, 8 maxima and 8 minima, from two univariate Gaussian distributions with means equal to +100 for maxima and to -100 for minima, respectively. The standard deviations of the two Gaussian distributions are the same and they are set equal to 50. To generate a function inside a cluster, we draw a random permutation of 8 elements and we reorder, according to this permutation, both the set of maxima and the set of minima associated to the cluster. Then, we take a regular grid of 16 nodes on the abscissa axis:



(a) The functions f_0 and f_3 belonging to the data set described in Appendix C.1. Note the changes, between f_0 and f_3 , in the disposition of the smaller peaks w.r.t. to the highest one.



(b) The merge trees (T_{f_0}, h_{f_0}) and (T_{f_3}, h_{f_3}) associated to the functions f_0, f_3 in Figure 8a. The changes in the tree structures reflect the different disposition of the disposition of the smaller peaks w.r.t. to the highest one in the associated functions.



(c) The persistence diagram representing the functions in Figure 8a and all the other functions produced in Appendix C.1. The point $(0,1)$ has multiplicity equal to the number of local minima minus 1.

(d) Matrix of pairwise distances of the merge trees obtained in Appendix C.1.

(e) Multidimensional Scaling Embedding in \mathbb{R}^2 of the matrix of pairwise distances shown in Figure 8d. The shades of gray describe, from white to black, the ordering of the trees.

Figure 8: Plots related to the simulated scenario presented in Appendix C.1.

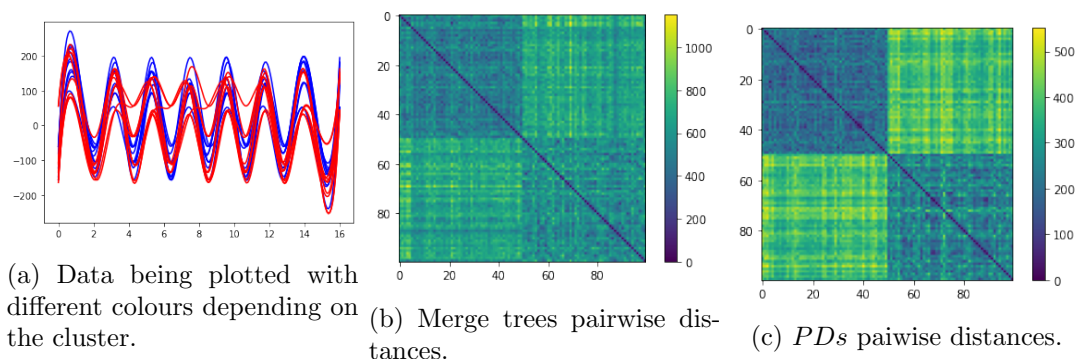


Figure 9: Example II. In the first row we can see few data from the two clusters. In the second row we see the matrices of pairwise distance extracted with trees and PDs . The data are ordered according to their cluster. It is clear how PDs perform much better in separating the two clusters.

on the ordinate axis we associate to the first point on the grid the first minimum, to the second the first maximum, to the third the second minimum and so on. To obtain a function we interpolate such points with a cubic spline. We thus generate 50 functions in each cluster. The key point is that, within the same cluster, the critical points are the same but for their order, while the two clusters correspond to two different sets of critical points.

In this example, we expect that the clustering structure carried by the amplitude of the functions will be shadowed by the differences in the merging order, when adopting the merge tree representation; while persistence diagrams should perform much better because they are less sensitive to peak reordering. This is in fact confirmed by inspecting the distance matrices in Figure 9b and Figure 9c.

C.3 Example III

Here we reverse the state of affairs and we set the feature for discriminating between clusters to be the merging structure of the functions. Hence, we generate two clusters of functions: the members of each cluster have the same merging structure which is however different between clusters.

To generate the two clusters of 50 functions each, we first draw an independent sample of 10 critical values, 10 maxima and 10 minima, shared between the clusters. Such samples are drawn from Gaussian distributions with means 100 and -100 respectively and standard deviation 200. Given a regular grid of 20 nodes on the abscissa axis, on the ordinate axis we associate to the first point of the grid a maximum, to the second a minimum, and so on, as is Example I. To generate every member of one cluster or the other, we add to the ordinate of each maximum or minimum critical point a random noise generated by a Gaussian with mean 0 and standard deviation 100. Then we reorder such points following a cluster-specific order. And, lastly, we interpolate with a cubic spline. We remark that the ordering of the maxima and that of the minima now becomes essential. For the two clusters, these orderings are fixed but different and they are set as follows (0 indicates the smallest value and 9 being the largest value):

- first cluster: maxima are ordered along the sequence (0, 1, 2, 3, 4, 5, 6, 7, 8, 9), minima along the sequence (0, 1, 2, 3, 4, 5, 6, 7, 8, 9);

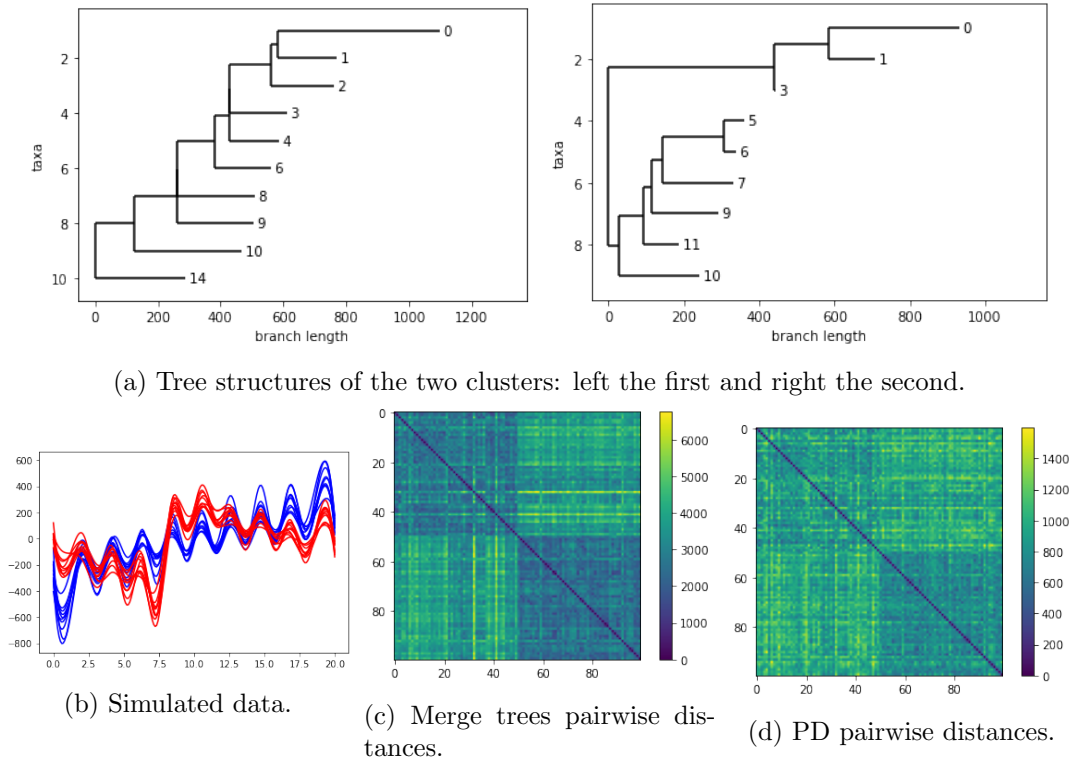


Figure 10: Example III. In the first row we can find the tree structures associated to the two clusters. In the second row, leftmost plot, we can see a few data from the two clusters. In the central and rightmost column of the second row we see the matrices of pairwise distances between merge tree representations and *PDs*, respectively. The data are ordered according to their cluster. It is clear how in this example merge trees are more suitable to separate the two clusters.

- second cluster: maxima are ordered along the sequence(3, 2, 1, 0, 8, 9, 7, 6, 4, 5), minima along the sequence (3, 2, 1, 0, 8, 9, 7, 6, 4, 5).

Such different orderings provide non-isomorphic tree structures for the merge trees associated to the functions of the two clusters, as we can see in Figure 10a, while keeping a similar structure in terms of persistence diagrams.

In this example, we expect *PDs* to be unable to recognise the clustering structure among the data; indeed, the only discriminant feature available to *PDs* is the different height of critical points, but this bears little information about the clusters.

We can visually observe this by comparing Figure 10c with Figure 10d.

Appendix D. Proofs

Proof of Theorem 6.

Let $f : X \rightarrow \mathbb{R}$ be a bounded function defined on a path connected topological space X and let $\varphi : Y \rightarrow X$ be an homeomorphism. We need to prove that the merge tree and the persistence diagram associated to the function f and $f' = f \circ \varphi$ are isomorphic.

We know that:

$$Y_t = \{f'^{-1}((-\infty, t])\} = \{y | f'(y) \leq t\} = \{x = \varphi(y) | f(x) \leq t\}$$

This means that $y \in Y_t$ if and only if $\varphi(y) \in X_t$, and so $Y_t = \varphi^{-1}(X_t)$. Since the restriction of an homeomorphism is still an homeomorphism, we can take its inverse, and by the composition properties of π_0 , we obtain that $\pi_0(X_t) \cong \pi_0(Y_t)$. Given $t' < t$, we thus have the following commutative diagram:

$$\begin{array}{ccc} X_{t'} & \longrightarrow & X_t \\ \downarrow \varphi & & \downarrow \varphi \\ Y_{t'} & \longrightarrow & Y_t \end{array}$$

and passing to path connected components/homology:

$$\begin{array}{ccc} \pi_0(X_{t'}) & \longrightarrow & \pi_0(X_t) \\ \downarrow \pi_0(\varphi) & & \downarrow \pi_0(\varphi) \\ \pi_0(Y_{t'}) & \longrightarrow & \pi_0(Y_t) \\ \\ H_p(X_{t'}) & \longrightarrow & H_p(X_t) \\ \downarrow H_p(\varphi) & & \downarrow H_p(\varphi) \\ H_p(Y_{t'}) & \longrightarrow & H_p(Y_t) \end{array}$$

where the vertical arrows in the second diagram are isomorphisms of groups. The first diagram then gives the isomorphism of merge trees, while the last one gives the isomorphism of $PD_0(f)$ and $PD_0(f')$. ■

Proof of Theorem 11.

Each leaf in (T, h_f) corresponds to a point in $PD(f)$. The x coordinate of each point is given by its height, which can be retrieved through h_f . Consider $v \in L_T$ and let γ_v , be the ordered set $\{v' \in V_T | v' \geq v\}$ i.e. the path from v towards r_T . The y coordinate of the points associated to v is the minimal height at which γ_v intersects another path γ_l , with l being a leaf with height less than v . ■

Proof of Theorem 12.

To prove the theorem, we need some notation and some auxiliary results. To avoid dealing with unpleasant technicalities we work under the hypothesis that for any merge tree (T, h) , h is an injective function. We call this assumption (G). It is not hard to see that for any fixed merge tree T , for any $\epsilon > 0$, there is a merge tree T' such that (G) holds and $d_E(T, T') \leq \epsilon$. It is enough to make arbitrarily small shrinkings to the edges. Similarly for functions: given a continuous function we can always find an arbitrarily close function - in terms of $\|\cdot\|_\infty$ - such that the associated merge tree (T, h_f) satisfies (G).

First we define the *least common ancestor* (LCA) of a set of vertices in a merge tree.

Definition 22 Given a merge tree (T, h_T) and set of vertices $A = \{a_1, \dots, a_n\} \subset V_T$, we define $LCA(a_1, \dots, a_n) = \min \bigcap_{i=1}^n \{v \in V_T \mid v \geq a_i\}$.

Consider now f, g tame functions on the path connected topological space X such that $\sup_{x \in X} |f(x) - g(x)| \leq \varepsilon$. Let (F, h_f) and (G, h_g) be their associated merge trees. For $t \in \mathbb{R}$, we set $X_t^f = f^{-1}((-\infty, t])$. Since $|f(x) - g(x)| \leq \varepsilon$ we have $X_t^f \subset X_{t+\varepsilon}^g$ and of course $X_t^g \subset X_{t+\varepsilon}^f$.

We set $f_t^{t+\varepsilon} := \pi_0(X_t^f \hookrightarrow X_{t+\varepsilon}^f)$, $g_t^{t+\varepsilon} := \pi_0(X_t^g \hookrightarrow X_{t+\varepsilon}^g)$, $\alpha_t^{t+\varepsilon} := \pi_0(X_t^f \hookrightarrow X_{t+\varepsilon}^g)$, and $\beta_t^{t+\varepsilon} := \pi_0(X_t^g \hookrightarrow X_{t+\varepsilon}^f)$. We then call $F_t := \pi_0(X_t^f)$ and $G_t := \pi_0(X_t^g)$. With these pieces of notation we can write down the following commutative diagram:

$$\begin{array}{ccccc} F_t & \xrightarrow{f_t^{t+\varepsilon}} & F_{t+\varepsilon} & \cdots & \rightarrow & F_{t'} & \xrightarrow{f_{t'}^{t'+\varepsilon}} & F_{t'+\varepsilon} \\ & \searrow & \nearrow & & & \searrow & \nearrow & \\ G_t & \xrightarrow{g_t^{t+\varepsilon}} & G_{t+\varepsilon} & \cdots & \rightarrow & G_{t'} & \xrightarrow{g_{t'}^{t'+\varepsilon}} & G_{t'+\varepsilon} \end{array}$$

Note that the diagonal maps are $\alpha : F_t \rightarrow G_{t+\varepsilon}$ and $\beta : G_t \rightarrow F_{t+\varepsilon}$. Lastly, if $a_t' = f_t^{t'}(a_t)$, we say that $a_t < a_{t'}$.

If we collect together the path connected components $\{F_t\}_{t \in \mathbb{R}}$ and $\{G_t\}_{t \in \mathbb{R}}$ taking the disjoint unions $\mathbf{F} := \coprod_{t \in \mathbb{R}} F_t$ and $\mathbf{G} := \coprod_{t \in \mathbb{R}} G_t$ we can write down the maps $\alpha : \mathbf{F} \rightarrow \mathbf{G}$ and $\beta : \mathbf{G} \rightarrow \mathbf{F}$, so that given $a_t \in F_t$, $\alpha(a_t) := \alpha_t^{t+\varepsilon}(a_t)$. Given $a_{t'} \in \mathbf{F}$, we also set $h_f(a_{t'}) = t'$. The same for h_g .

We point out that the vertices of the merge trees F and G are contained in some F_t or G_t , respectively, and thus we have $V_F \hookrightarrow \mathbf{F}$ and $V_G \hookrightarrow \mathbf{G}$. We will often refer to $v \in V_F$ as $v \in \mathbf{F}$, and thus, for instance, take $\alpha(v)$, without explicitly mentioning the inclusion map. Note that the partial order we defined for \mathbf{F} and \mathbf{G} is compatible the the one of the vertices of the merge trees.

In a more technical language, \mathbf{F} and \mathbf{G} are the display posets of the two persistence sets $\pi_0(X^f)$ and $\pi_0(X^g)$ (Curry et al., 2022), but we want to avoid introducing such technical definitions. The work of Beketayev et al. (2014) shows that α and β give an ε -interleaving of merge trees (see Beketayev et al. (2014)), which, by Agarwal et al. (2018), is equivalent to the map α satisfying the following conditions:

- (P1) $h_g(\alpha(a_t)) = h_f(a_t) + \varepsilon = t + \varepsilon$ for all $a_t \in \mathbf{F}$
- (P2) if $\alpha(a_t) < \alpha(a_{t'})$ then there is $a_{t''}$ such that $a_t < a_{t''}$, $a_{t'} \leq a_{t''}$ and $t'' - t' < \varepsilon$.
- (P3) if $b_{t'} \in \mathbf{G} - \alpha(\mathbf{F})$, then, given $b_t = \min\{b_{t''} > b_{t'} \mid b_{t''} \in \alpha(\mathbf{F})\}$, we have $t - t' \leq 2\varepsilon$.

A map which satisfies (P1)-(P3) is called ε -good (Agarwal et al., 2018).

To bridge between the continuous nature of \mathbf{F} and \mathbf{G} and the discrete (F, h_f) and (G, h_g) , we define the following maps:

$$L_f : \mathbf{F} \rightarrow V_F$$

$L_f(a_t) = \max\{v \in V_F \mid v \leq a_t\}$ and similarly for L_g . Leveraging on these definitions we set $\phi := L_g \circ \alpha$ and $\psi := L_f \circ \beta$.

Finally we start building an edit path between (F, h_f) and (G, h_g) . To do so we progressively add couples to an empty set M : couples of the form $(v, "D")$ mean that the vertex $v \in V_F$ is deleted, while $(v, "D"), w$ means that $w \in V_G$ is deleted, $(v, "G")$ means

that the vertex $v \in V_F$ is ghosted, $(\text{"}G\text{"}, w)$ means that $w \in V_G$ is ghosted and (v, w) means that we shrink $(v, \text{father}(v))$ so that the weight of $(v, \text{father}(v))$ becomes equal to the one of $(w, \text{father}(w))$. The set M is in very close analogy with the *mappings* defined in Pegoraro (2024b).

By working simultaneously on F and G , we collect all the “edits” in $M \subset V_F \cup \{\text{"}D\text{"}, \text{"}G\text{"}\} \times V_G \cup \{\text{"}D\text{"}, \text{"}G\text{"}\}$ and then, in the last subsection of the proof, we use M on induce an edit path between F and G . We will call $\pi_F : M \rightarrow V_F \cup \{\text{"}D\text{"}, \text{"}G\text{"}\}$ the projection on the first factor, and π_G the projection on the second.

Appendix E. Leaves of F

In this section we take care of the leaves of the merge tree F .

E.1 Selecting the Coupled Leaves

Consider the following set of leaves:

$$\mathcal{L}_F = \{v \in L_F \mid \nexists v' \in L_F \text{ such that } \alpha(v) < \alpha(v')\} \quad (4)$$

We give a name to the condition used to assert if for a vertex $v \in L_F$, we have $v \in \mathcal{L}_F$:

$$(a) \nexists v' \in L_F \text{ such that } \alpha(v) < \alpha(v')$$

so that we can more easily refer to it during the proof. Observe that we never have $\alpha(v) = \alpha(v')$ thanks to condition (G).

The set \mathcal{L}_F is the set of leaves which will be coupled by M : we add to M all the couples of the form $(v, \phi(v))$ with $v \in \mathcal{L}_F$ and add $(v, \text{"}D\text{"})$ for all $v \in L_F - \mathcal{L}_F$.

Lemma 23 *Given $v, v' \in L_F$, then $\phi(v) \geq \phi(v')$ if and only if $v = v'$. Moreover, for every $v' \in L_F$ for which (a) does not hold, there is $v \in \mathcal{L}_F$ such that $\alpha(v) < \alpha(v')$.*

Proof *The first part of the proof reduces to observing that $\phi(v) \leq \phi(v')$ if and only if $\alpha(v) \leq \alpha(v')$.*

Now consider $v' \in L_F$ such that (a) does not hold. We know there is v_0 such that $\alpha(v_0) < \alpha(v')$. If $v_0 \in \mathcal{L}_F$ we are done, otherwise there is v_1 such that $\alpha(v_1) < \alpha(v_0) < \alpha(v')$. Note that $f(v_1) < f(v_0)$. Thus we can carry on this procedure until we find $v_i \in \mathcal{L}_F$. Note that $\arg \min_{a \in V_F} f(a) \in \mathcal{L}_F$, thus, in a finite number of steps we are done. ■

E.2 Height Bounds on Couples

Now we want to prove the following proposition which will be used to give an upper bound for the cost of the edits induced by the couples $(v, \phi(v))$ added to M .

Lemma 24 *Given $v \in \mathcal{L}_F$, then $|h_f(v) - h_g(\phi(v))| \leq \varepsilon$.*

Proof *Suppose the thesis does not hold. Since $h_g(\phi(v)) \leq h_f(v) + \varepsilon$, contradicting the thesis means that we have $v \in \mathcal{L}_F$ such that:*

$$(b) h_f(v) - h_g(\phi(v)) > \varepsilon.$$

Let $w = \phi(v)$. If (b) holds, then $h_g(\text{father}(w)) - h_g(w) > h_g(\alpha(v)) - h_g(w) > 2\varepsilon$. Let $v' = \psi(w) \leq \beta(w)$. Note that $h_f(v') < h_f(v)$. We have $\phi(v') \leq \alpha(v') \leq \alpha(\beta(w))$. But since $h_g(\text{father}(w)) - h_g(w) > 2\varepsilon$, we also have $\alpha(v') \leq \alpha(v)$ with $v' \neq v$ which is absurd by Theorem 23. ■

E.3 Cost Bound on Deletions

In this step we prove a cost bound for some the vertices of F which are going to be deleted. We add to M the couples $(x, "D")$ for every $x \notin \{v' > v \mid v \in \mathcal{L}_F\}$.

Lemma 25 *Given $x \notin \{v' \in V_F \mid \exists v < v', v \in \mathcal{L}_F\}$, then $w_F((x, \text{father}(x))) \leq 2\varepsilon$.*

Proof *We simply observe that, if $x \notin \{v' \in V_F \mid \exists v < v', v \in \mathcal{L}_F\}$ then there is $v \in \mathcal{L}_F$ such that $\alpha(v) < \alpha(x)$. By property (P2) of α , since $h_f(v) < h_f(x)$, we have that $(x, "D")$ has cost at most 2ε . ■*

Appendix F. Leaves and deletions of G

Similarly we add to M the couples $(y, "D")$ for every $y \notin \{w' \in V_G \mid \exists w < w', w \in \pi_G(M) \cap V_G\}$.

Lemma 26 *Given $y \in V_G$ such that $y \notin \{w' \in V_G \mid \exists w < w', w \in \pi_G(M) \cap V_G\}$, then $w_G((y, \text{father}(y))) \leq 2\varepsilon$.*

Proof *Consider $\beta(y)$. Let $v \leq \beta(y)$ leaf. We have $\alpha(\beta(y)) \geq \alpha(v)$ and $\alpha(\beta(y)) \geq y$. If $L_g(\alpha(\beta(y))) \neq y$ we are done since $h_g(\alpha(\beta(y))) = h_g(y) + 2\varepsilon$. Suppose instead $L_g(\alpha(\beta(y))) = y$. We know that there is always $v_0 \in \mathcal{L}_F$ such that $\alpha(v_0) \leq \alpha(v)$ (either $v \notin \mathcal{L}_F$ or $v = v_0$). Suppose $\alpha(v_0) \geq y$. Since $\alpha(\beta(y)) \geq \alpha(v) \geq \alpha(v_0)$, then $L_g(\alpha(v_0)) = y$ and so $y \in \pi_G(M)$. Which is absurd.*

Thus, we are left with $\alpha(v_0) \leq y$. But this is absurd as well as it implies again $y \in \{w' \in V_G \mid \exists w < w', w \in \pi_G(M) \cap V_G\}$. ■

Appendix G. Internal Vertices

Now we want to take into account the internal vertices of F and G .

Thanks to Theorem 25 and Theorem 26 we can delete all $x \notin \{v' \in V_F \mid \exists v < v', v \in \mathcal{L}_F\}$ and $y \in V_G$ such that $y \notin \{w' \in V_G \mid \exists w < w', w \in \pi_G(M) \cap V_G\}$, each with cost at most 2ε . Note that these deletions do not change the heights of any non deleted vertex.

Call F_1 and G_1 the two trees obtained after such deletions and after the ghosting of all the order 2 vertices arising - and consequently adding $(v, "G")$ or $(y, "G")$ to M for all the ghosted vertices respectively in F or G . If we consider $\alpha|_{\mathbf{F}_1}$ then by construction $\alpha|_{\mathbf{F}_1} : \mathbf{F}_1 \rightarrow \mathbf{G}_1$. Similarly $\beta|_{\mathbf{G}_1} : \mathbf{G}_1 \rightarrow \mathbf{F}_1$. Moreover $\alpha(\mathbf{F}) = \alpha|_{\mathbf{F}_1}(\mathbf{F}_1)$. Thus $\alpha|_{\mathbf{F}_1}$ is still ε -good. In what follows, with an abuse of notation, we avoid explicitly writing the restriction of the maps α and β , implying that these are always considered as defined on the "pruned" trees F_1 and G_1 .

G.1 Results on Internal vertices

We prove the following results.

Lemma 27 *Let $x \in V_{F_1} - L_{F_1}$ such that $x = LCA(A)$ with $A = \{v \in V_{F_1} \mid v < x\} \cap L_{F_1}$. Let $y = LCA(\phi(A))$. Then $|h_f(x) - h_g(y)| \leq \varepsilon$.*

Proof *For every $a \in A$ we know $\phi(a) < \phi(x)$ and thus $y \leq \phi(x)$. Thus $h_g(y) \leq h_f(x) + \varepsilon$. Suppose then $h_g(y) < h_f(x) - \varepsilon$. However, $\beta(y) \geq x$ for $\beta(y) \geq \beta(\phi(a)) \geq a$. Which is absurd for $h_f(\beta(y)) = h_g(y) + \varepsilon < h_f(x)$. ■*

Lemma 28 Let $x \in V_{F_1} - L_{F_1}$ such that $x = LCA(A)$ with $A = \{v \in V_{F_1} \mid v < x\} \cap L_{F_1}$. Let $y = LCA(\phi(A)) = LCA(B)$ with $B = \{w \in V_{G_1} \mid w < y\} \cap L_{G_1}$.

Then for every $w = \phi(v) \in B - \phi(A)$, let $x' = LCA(A \cup \{v\})$. Then we have $h_f(x') - h_f(x) \leq 2\varepsilon$.

Proof Since $v \not\leq x$ but $\phi(v) < \phi(x)$, we know $\min\{h_f(x') - h_f(x), h_f(x') - h_f(x)\} \leq 2\varepsilon$. Suppose $h_f(x') - h_f(x) > 2\varepsilon$. We know $\beta(\alpha(x)) > v$ for $\phi(x) > \phi(v)$. But then $\beta(\alpha(x)) \geq x'$ which is absurd since $h_f(\beta(\alpha(x))) = h_f(x) + 2\varepsilon < h_f(x')$. ■

Lemma 29 Consider $e = (x, \text{father}(x)) \in E_{F_1}$, $x = LCA(A)$ with $A = \{v \in V_{F_1} \mid v < x\} \cap L_{F_1}$. Let $y = LCA(\phi(A)) = LCA(B)$, with $B = \{w \in V_{G_1} \mid w < y\} \cap L_{G_1}$. Let $e' = (y, \text{father}(y)) \in E_{G_1}$. Then $|w_{F_1}(e) - w_{G_1}(e')| \leq 2\varepsilon$.

Proof We know by Theorem 27 that $|h_f(x) - h_g(y)| \leq \varepsilon$. Thus we can focus on $x' = \text{father}(x)$ and $y' = \text{father}(y)$. Let $A' = \{v \in V_{F_1} \mid v < x'\} \cap L_{F_1}$, $B' = \{w \in V_{G_1} \mid w < y'\} \cap L_{G_1}$, $w = LCA(\phi(A'))$ and $v = LCA(\psi(B'))$. By Theorem 27, again $|h_f(x') - h_g(w)| \leq \varepsilon$ and $|h_f(v) - h_g(y')| \leq \varepsilon$.

Since $A \subset A'$, then $B \subset \phi(A')$ and similarly $A \subset \psi(B')$. Which entails $x' \leq v$ and $y' \leq w$. Since $x'' = LCA(\psi(\{w' \in V_{G_1} \mid w' < w\})) \geq v$, by Theorem 28 we have $h_f(v) - h_f(x') \leq 2\varepsilon$ and, similarly, $h_g(w) - h_g(y') \leq 2\varepsilon$. Putting together $|h_f(x') - h_g(w)| \leq \varepsilon$, $y' < w$ and $h_g(w) - h_g(y') \leq 2\varepsilon$ and the analogous inequalities for y' we obtain $|h_f(x') - h_g(y')| \leq \varepsilon$.

Thus $|h_f(x') - h_f(x) - (h_g(y') - h_g(y))| \leq 2\varepsilon$. ■

G.2 Deleting Internal Vertices

Now we proceed as follows: for every $x \in V_{F_1}$ let $A = \{v \in V_{F_1} \mid v < x\} \cap L_{F_1}$, $y = LCA(\phi(A)) = LCA(B)$, with $B = \{w \in V_{G_1} \mid w < y\} \cap L_{G_1}$. If $B \neq \phi(A)$, then add $(x, "D")$ to M and delete x . By Theorem 28 the cost of deleting x is less than 2ε . We do so for all $x \in V_{F_1}$. Then we follow an analogous process for $y \in V_{G_1}$: let $y = LCA(B)$ with $B = \{w \in V_{G_1} \mid w < y\} \cap L_{G_1}$, $x = LCA(\psi(B)) = LCA(A)$ with $A = \{v \in V_{F_1} \mid v < x\} \cap L_{F_1}$. If $A \neq \psi(B)$, then add $(\text{"D"}, y)$ to M and delete y . By Theorem 28 the cost of deleting y is less than 2ε .

G.3 Coupling the Internal Vertices

After the deletions in Appendix G.2 we obtain two merge trees F_2 and G_2 , with the same leaves as F_1 and G_1 but with the property that for each $x \in V_{F_2}$ we have a bijection between the leaves $A = \{v \in V_{F_1} \mid v < x\} \cap L_{F_1}$ and the leaves in $\text{sub}_{G_2}(y)$ with $y = LCA(\phi(A))$. Thus for any edge $(x, x') \in E_{F_2}$ we have a unique edge $(y, y') \in E_{G_2}$ such that the leaves of $\text{sub}_{F_2}(x)$ and $\text{sub}_{G_2}(y)$ are in bijection and the same for x' and y' . Thus we can couple x and y , add (x, y) to M and make the shrinking to pair their weights. Since deleting a vertex doesn't affect the weight of the other edges, then we can still apply Theorem 29 which guarantees that the shrinkings cost less than 2ε .

Appendix H. Inducing the Edit Path

To conclude the proof we sum up everything and induce and order edits operations according to the couples contained in M , so that the costs of the edits matches the ones described along the previous subsections of the proof.

First we apply all the deletions on F described in Appendix E.3, with the cost of every edit being at most 2ε . Then we ghost all order 2 vertices. By construction we obtain, from F , the tree F_1 . At this point we delete internal vertices of F_1 according to the procedure described in Appendix G.2, obtaining F_2 . Then we shrink all the edges of F_2 , according to Appendix G.3, obtaining G_2 . Then we insert all the edges needed to obtain G_1 from G_2 , which are associated to the couples (D, y) mentioned in Appendix G.2. Then we go on with the splittings induced by $(G, w) \in M$, which are needed to subsequently insert the edges which take us from G_1 to G , as explained in Appendix F. In the respective sections it is shown that all the edits we employed have cost less than 2ε .

This concludes the proof. ■

Proof of Theorem 16.

We build an edit path γ_g between T_f and T_g as in Theorem 12. Then we define T' and the merge tree obtained from T_g applying only the deletions contained in γ_g which deletes leaves of T_g .

Note that, at this point, the number of leaves in T' cannot be bigger than the number of leaves in T_f . Thus, if we name C_f the number of leaves in T_f , we have $\#E_{T_f}, \#E_{T'} \leq 2C_f$. And so:

$$d_E(T_f, T') \leq 4C_f \|f - g\|_\infty. \quad (5)$$

Now, to obtain T' from T_g , we need to remove a certain number of leaves from T_g , deleting the edge connecting each selected leaf with its father. We recall that each leaf is associated to a local minimum of g , and every father of a leaf is a local maximum of g .

Thus, there exist x_1, \dots, x_{2n} ordered local minima and local maxima points of g . WLOG suppose x_{2i+1} are local minima and x_{2i} are local maxima. Let W be the set of indexes i such that x_{2i+1} is a local minimum associated to a leaf deleted from T_g . We know that for every such x_{2i+1} , there is a local maximum \tilde{x}_{2i+1} its father. Thus, we have:

$$d_E(T', T_g) \leq \sum_{i \in W} |g(\tilde{x}_{2i+1}) - g(x_{2i+1})| \leq A := \sum_{j=1, \dots, 2n-1} |g(x_{j+1}) - g(x_j)|.$$

Now, consider the partition of $[a, b]$ given by the union of the critical points of f , $\{z_1, \dots, z_k\}$, with $\{x_1, \dots, x_{2n}\}$, called $\{y_1, \dots, y_m\}$. Note that $k \leq 2C_f$. We know that:

$$V_{[a,b]}(f) = \sum_{i=1}^k (-1)^{i+1} (f(z_{i+1}) - f(z_i))$$

If we define:

$$B := \sum_{i=1}^k |(g(z_{i+1}) - g(z_i))| \leq V_{[a,b]}(g),$$

we know:

$$|B - V_{[a,b]}(f)| \leq 4C_f \|f - g\|_\infty.$$

Now, suppose that, in the sequence $\{y_1, \dots, y_m\}$, we have the following situation:

$$z_i \leq x_j < x_{j+1} < \dots < x_{j+q} \leq z_{i+1}.$$

To lighten the notation, suppose $\|f - g\|_\infty \leq \varepsilon$.

By construction x_{2j+1} is a local minima of g , and so is associated to a leaf in T_g , and we call \tilde{x}_{2j+1} the local maxima of g associated to its father in T_g . Moreover, either $\tilde{x}_{2j+1} = x_{2j}$ or $\tilde{x}_{2j} = x_{2j+2}$, and, in particular:

$$g(x_{2j+1}) < g(x_{2j}), g(x_{2j+2}) \leq g(\tilde{x}_{2j+1}),$$

and

$$g(x_{2j+1}) < g(\tilde{x}_{2j+1}) + 2\varepsilon.$$

Lastly, any $z_i \in (x_{j-1}, x_j)$ cannot be a critical point for g and, replacing $g(z_i)$ with $g(x_{j-1})$ or $g(x_j)$ causes an error of at most 2ε .

Thus:

$$\begin{aligned} |g(z_i) - g(x_j)| + \sum_{r=0}^{q-1} |g(x_{j+r}) - g(x_{j+r+1})| + |g(z_{i+1}) - g(x_{j+q})| \leq \\ |g(z_i) - g(z_{i+1})| + |g(x_{j+q}) - g(x_j)| + \sum_{r=0}^{q-1} |g(x_{j+r}) - g(x_{j+r+1})| + 4\varepsilon. \end{aligned}$$

This means that we can write:

$$|C - (A + B)| \leq 4C_f \varepsilon,$$

with $C := |\sum_{i=1}^m (g(y_{i+1}) - g(y_i))|$. In particular, this entails:

$$A \leq C - B + 4C_f \varepsilon \leq V_X(g) - B + 2C_f \varepsilon,$$

as, by construction, $V_{[a,b]}(g) \geq C \geq B$. But:

$$V_{[a,b]}(g) - B \leq |V_{[a,b]}(g) - V_{[a,b]}(f)| + |V_{[a,b]}(f) - B|.$$

Thus:

$$A \leq |V_{[a,b]}(g) - V_{[a,b]}(f)| + 4C_f \|f - g\|_\infty.$$

Putting the pieces together:

1. $d_E(T_f, T') \leq 4C_f \|f - g\|_\infty$;
2. $d_E(T', T_g) \leq |V_{[a,b]}(g) - V_{[a,b]}(f)| + 4C_f \|f - g\|_\infty$.

Thus, via triangular inequality we conclude the proof. ■

Proof of Theorem 18.

By Theorem 16 and Theorem 17 we know:

$$d_E(T_f, T_{\hat{f}_n}) \leq 8C_f \|f - \hat{f}_n\|_\infty + (b - a) \|Df - D\hat{f}_n\|_\infty.$$

With C_f being the number of local minima points in f . Thus:

$$\begin{aligned} P(d_E(T_f, T_{\hat{f}_n}) \leq 2\varepsilon) &\geq P(\|f - \hat{f}_n\|_\infty \leq 8C_f \varepsilon) \cdot P(\|Df - D\hat{f}_n\|_\infty \leq (b - a)\varepsilon) \\ &\geq 1 - h_n(8C_f \varepsilon) - g_n((b - a)\varepsilon) + h_n(8C_f \varepsilon)g_n((b - a)\varepsilon), \end{aligned}$$

which is our thesis. ■

Proof of Theorem 19.

1. On every interval $[z_i, z_{i+1}]$ we have $|f(z_i) - f(x)| \leq L \cdot |z_i - x|$ and $|f_\delta^{PL}(z_i) - f_\delta^{PL}(x)| \leq L_i \cdot |z_i - x|$ with $L_i = |f_\delta^{PL}(z_{i+1}) - f_\delta^{PL}(z_i)| / (z_{i+1} - z_i)$. At the same time, we have that $|f_\delta^{PL}(z_{i+1}) - f_\delta^{PL}(z_i)| / (z_{i+1} - z_i) = |(z_{i+1} - z_i)| / (z_{i+1} - z_i) \leq L$. Thus, for $x \in (z_i, z_{i+1})$ we have:

$$|f(x) - f_\delta^{PL}(x)| \leq |f(x) - f(z_i)| + |f_\delta^{PL}(x) - f_\delta^{PL}(z_i)| \leq 2L(z_{i+1} - z_i).$$

2. To prove this point, we make use of the following result, which we adapt from Theorem 3.4.1 in Quarteroni and Valli (2008).

Theorem 30 (adapted from Quarteroni and Valli (2008)) Fix $\{z_1 = a, \dots, z_m = b\} \subset X = [a, b]$, increasing sequence of numbers and let $\delta = \max z_{i+1} - z_i$. There exist a constant $A > 0$ such that for every $f \in H^2([a, b])$, its piecewise linear interpolant f_δ^{PL} on $\{z_i\}_{i=1, \dots, m}$, satisfies for every $i = 1, \dots, m - 1$:

$$\int_{z_i}^{z_{i+1}} |f - f_\delta^{PL}|^2 dx \leq A^2 \delta^4 \int_{z_i}^{z_{i+1}} |D^2 f|^2 dx, \quad (6)$$

and

$$\int_{z_i}^{z_{i+1}} |Df - Df_\delta^{PL}|^2 dx \leq A^2 \delta^2 \int_{z_i}^{z_{i+1}} |D^2 f|^2 dx. \quad (7)$$

By Theorem 30, we have that:

$$\|Df - Df_\delta^{PL}\|_2^2 \leq A^2 \delta^2 \|D^2 f\|_2^2.$$

By Holder inequality we then obtain:

$$\|Df - Df_\delta^{PL}\|_1 \leq (b - a)^{1/2} A \delta \|D^2 f\|_2.$$

Thus $V(f - f_\delta^{PL}) \leq (b - a)^{1/2} A \delta \|D^2 f\|_2$.

3. Putting the pieces together and using Theorem 16:

$$d_E(T_f, T_{f_\delta^{PL}}) \leq 16C_f L \delta + (b - a)^{1/2} A \delta \|D^2 f\|_2.$$

This concludes the proof. ■

Proof of Theorem 20.

We have:

$$\|f - \hat{f}_{n,m}^{PL}\|_\infty \leq \|f - \hat{f}_n\|_\infty + 2 \|Df\|_\infty \frac{b-a}{m}.$$

Similarly:

$$\begin{aligned} V(f - \hat{f}_{n,m}^{PL}) &\leq V(f - \hat{f}_n) + (b-a)^{3/2} \frac{A}{m} (\|D^2 \hat{f}_n\|_2 + \varepsilon) \leq \\ &V(f - \hat{f}_n) + (b-a)^{3/2} \frac{A}{m} (\|D^2 \hat{f}_n - D^2 f\|_2 + \|D^2 f\|_2) \leq \\ &\|Df - D\hat{f}_n\|_\infty (b-a) + (b-a)^2 \frac{A}{m} (\|D^2 \hat{f}_n - D^2 f\|_\infty + \|D^2 f\|_\infty) \leq \\ &C' \cdot \|Df - D\hat{f}_n\|_\infty + C'' \frac{\|D^2 \hat{f}_n - D^2 f\|_\infty}{m} + \frac{C'''}{m}, \end{aligned}$$

for some constants $C', C'', C''' > 0$, and with A being the constant as in Theorem 30. Thus, for some constants C_1, \dots, C_4 , we have:

$$d_E(T_f, T_{\hat{f}_{n,m}^{PL}}) \leq C_1 \|f - \hat{f}_n\|_\infty + C_2 \|Df - D\hat{f}_n\|_\infty + C_3 \frac{\|D^2 \hat{f}_n - D^2 f\|_\infty}{m} + \frac{C_4}{m}.$$

The constants, in particular, are:

- $C_1 = 8C_f$;
- $C_2 = (b - a)$;
- $C_3 = (b - a)^2 A$;
- $C_4 = (b - a)(2 \|Df\|_\infty + (b - a)A \|D^2 f\|_\infty)$;

where C_f is number of local minima of f .

To conclude, if $m > C_4/\varepsilon$ we have:

$$P(d_E(T_f, T_{\hat{f}_{n,m}^{PL}}) < 4\varepsilon) \geq (1 - h_n(C_1\varepsilon))(1 - g_n(C_2\varepsilon))(1 - q_n(C_3\varepsilon/m)),$$

ending the proof. ■

Appendix I. Combining Metrics

To aggregate curvature and radius, we make use of the following proposition.

Proposition 31 *Given (X, d_0) and (X, d_1) metric spaces, then $d_{a,b,p} := (a \cdot d_0^p + b \cdot d_1^p)^{1/p}$, with $a, b \in \mathbb{R}_{>0}$ and $p \geq 1$, is a metric on X .*

Proof

$$d_{a,b,p}(x, y) = \|(a^{1/p} \cdot d_0(x, y), b^{1/p} \cdot d_1(x, y))\|_p.$$

Since, given $k > 0$, $k \cdot d_i$ is a metric if and only if d_i is a metric, we can rescale d_0 and d_1 and take $a = b = 1$. We refer to $d_{1,1,p}$ as d_p .

So:

- $d_p(x, y) = 0$ iff $d_0(x, y) = 0 = d_1(x, y)$ and this happens if and only if $x = y$.
- symmetry is obvious
- we use $\|h+q\|_p \leq \|h\|_p + \|q\|_p$ with $h = (d_0(x, z), d_1(x, z))$ and $q = (d_0(z, y), d_1(z, y))$.

Since $d_i(x, y) \leq d_i(x, z) + d_i(z, y)$ we get:

$$\|(d_0(x, y), d_1(x, y))\|_p \leq \|(d_0(x, z) + d_0(z, y), d_1(x, z) + d_1(z, y))\|_p = \|(d_0(x, z), d_1(x, z)) + (d_0(z, y), d_1(z, y))\|_p \leq \|(d_0(x, z), d_1(x, z))\|_p + \|(d_0(z, y), d_1(z, y))\|_p.$$

Therefore:

$$d_p(x, y) \leq d_p(x, z) + d_p(z, y).$$

■

References

- H. Adams, Tegan Emerson, M. Kirby, R. Neville, C. Peterson, P. Shipman, Sofya Chepushtanova, E. Hanson, F. Motta, and Lori Ziegelmeier. Persistence images: A stable vector representation of persistent homology. *Journal of Machine Learning Research*, 18(1):1–35, 2017.
- Pankaj K. Agarwal, Kyle Fox, Abhinandan Nath, Anastasios Sidiropoulos, and Yusu Wang. Computing the gromov-hausdorff distance for metric trees. *ACM Trans. Algorithms*, 14(2), apr 2018.
- Hiroshi Akima. On estimating partial derivatives for bivariate interpolation of scattered data. *The Rocky Mountain journal of mathematics*, pages 41–52, 1984.
- Mukund Balasubramanian and Eric L Schwartz. The isomap algorithm and topological stability. *Science*, 295(5552):7–7, 2002.
- Kenes Beketayev, Damir Yeliussizov, Dmitriy Morozov, Gunther H. Weber, and Bernd Hamann. Measuring the distance between merge trees. In *Topological Methods in Data Analysis and Visualization*, pages 151–166. Springer International Publishing, Cham, 2014.
- Satarupa Bhattacharjee and Hans-Georg Müller. Geodesic mixed effects models for repeatedly observed/longitudinal random objects. *arXiv preprint arXiv:2307.05726*, 2023.
- Subhrajit Bhattacharya, Robert Ghrist, and Vijay Kumar. Persistent homology for path planning in uncertain environments. *IEEE Transactions on Robotics*, 31(3):1–13, 2015.
- Silvia Biasotti, Daniela Giorgi, Michela Spagnuolo, and Bianca Falcidieno. Reeb graphs for shape analysis and applications. *Theoretical Computer Science*, 392(1-3):5–22, 2008.
- Philip Bille. A survey on tree edit distance and related problems. *Theoretical Computer Science*, 337(1-3):217 – 239, 2005.
- Omer Bobrowski, Sayan Mukherjee, and Jonathan E Taylor. Topological consistency via kernel estimation. *Bernoulli*, pages 288–328, 2017.
- Peter Bubenik. Statistical topological data analysis using persistence landscapes. *Journal of Machine Learning Research*, 16(3):77–102, 2015.
- Probal Chaudhuri and James S Marron. Sizer for exploration of structures in curves. *Journal of the American Statistical Association*, 94(447):807–823, 1999.
- F. Chazal, Brittany Terese Fasy, F. Lecci, A. Rinaldo, and L. Wasserman. Stochastic convergence of persistence landscapes and silhouettes. *Journal of Computational Geometry*, 6(2):140–161, 2015.
- Frédéric Chazal, Vin De Silva, Marc Glisse, and Steve Oudot. *The structure and stability of persistence modules*. Springer, 2016.
- Moo K. Chung, Peter Bubenik, and Peter T. Kim. Persistence diagrams of cortical surface data. In *Information Processing in Medical Imaging*, pages 386–397. Springer Berlin Heidelberg, 2009.
- D. Cohen-Steiner, H. Edelsbrunner, and J. Harer. Stability of persistence diagrams. *Discrete & Computational Geometry*, 37:103–120, 2007.

- Justin Curry, Jordan DeSha, Adélie Garin, Kathryn Hess, Lida Kanari, and Brendan Mallery. From trees to barcodes and back again ii: Combinatorial and probabilistic aspects of a topological inverse problem. *arXiv*, 2107.11212, 2021.
- Justin Curry, Haibin Hang, Washington Mio, Tom Needham, and Osman Berat Okutan. Decorated merge trees for persistent topology. *Journal of Applied and Computational Topology*, 2022.
- Vin De Silva, Elizabeth Munch, and Amit Patel. Categorized reeb graphs. *Discrete & Computational Geometry*, 55(4):854–906, 2016.
- M Delecroix and AC Rosa. Nonparametric estimation of a regression function and its derivatives under an ergodic hypothesis. *Journal of Nonparametric Statistics*, 6(4):367–382, 1996.
- I. L. Dryden and K. V. Mardia. *Statistical Shape Analysis*. Wiley, Chichester, 1998.
- Paromita Dubey and Hans-Georg Müller. Modeling time-varying random objects and dynamic networks. *Journal of the American Statistical Association*, 117(540):2252–2267, 2022.
- H. Edelsbrunner, D. Letscher, and A. Zomorodian. Topological persistence and simplification. *Discrete & Computational Geometry*, 28:511–533, 2002.
- Herbert Edelsbrunner and John Harer. Persistent homology—a survey. In *Surveys on discrete and computational geometry*, volume 453 of *Contemporary Mathematics*, pages 257–282. American Mathematical Society, Providence, RI, 2008.
- Y. Elkin and V. Kurlin. The mergegram of a dendrogram and its stability. *ArXiv*, 2007.11278v1 [cs.CG], 2020.
- Jianqing Fan. *Local polynomial modelling and its applications: monographs on statistics and applied probability 66*. Routledge, 2018.
- Brittany Terese Fasy, Fabrizio Lecci, Alessandro Rinaldo, Larry Wasserman, Sivaraman Balakrishnan, and Aarti Singh. Confidence sets for persistence diagrams. *The Annals of Statistics*, 42(6):2301–2339, 2014.
- Frédéric Ferraty and Philippe Vieu. *Nonparametric functional data analysis: theory and practice*. Springer Verlag, NY, 2006.
- Ellen Gasparovic, E. Munch, S. Oudot, Katharine Turner, B. Wang, and Yusu Wang. Intrinsic interleaving distance for merge trees. *ArXiv*, 1908.00063v1[cs.CG], 2019.
- Irène Gijbels and A-C Goderniaux. Data-driven discontinuity detection in derivatives of a regression function. *Communications in Statistics-Theory and Methods*, 33(4):851–871, 2005.
- Ulf Grenander. *General Pattern Theory: A Mathematical Theory of Regular Structures*. Oxford University Press, Oxford, 1993.
- Allen Hatcher. *Algebraic topology*. Cambridge University Press, Cambridge, 2000.

- Eunpyeong Hong, Y. Kobayashi, and A. Yamamoto. Improved methods for computing distances between unordered trees using integer programming. In *Combinatorial Optimization and Applications*, volume 10628 of *Lecture Notes in Computer Science*, pages 45–60. Springer International Publishing, Cham, 2017.
- Lida Kanari, Adélie Garin, and Kathryn Hess. From trees to barcodes and back again: Theoretical and statistical perspectives. *Algorithms*, 13(12), 2020.
- Göran Kauermann and JD Opsomer. Generalized cross-validation for bandwidth selection of backfitting estimates in generalized additive models. *Journal of Computational and Graphical Statistics*, 13(1):66–89, 2004.
- Miroslav Kramár, Arnaud Goulet, Lou Kondic, and K Mischaikow. Persistence of force networks in compressed granular media. *Physical review. E, Statistical, nonlinear, and soft matter physics*, 87:042207, 2013.
- Barry Lavine and Jerome Workman. Chemometrics. *Analytical chemistry*, 80(12):4519–4531, 2008.
- Yu Liu and Kris De Brabanter. Smoothed nonparametric derivative estimation using weighted difference quotients. *Journal of Machine Learning Research*, 21(65):1–45, 2020.
- Zhan-Qian Lu. Multivariate locally weighted polynomial fitting and partial derivative estimation. *journal of multivariate analysis*, 59(2):187–205, 1996.
- Saunders Mac Lane. *Categories for the Working Mathematician*. Springer New York, NY, Springer Science+Business Media New York 1978, 1998.
- YP Mack and Hans-Georg Müller. Derivative estimation in nonparametric regression with random predictor variable. *Sankhyā: The Indian Journal of Statistics, Series A*, pages 59–72, 1989.
- J. S. Marron, J. Ramsay, L. Sangalli, and A. Srivastava. Statistics of time warpings and phase variations. *Electronic Journal of Statistics*, 8(2):1697–1702, 2014.
- J. S. Marron, J. Ramsay, L. Sangalli, and A. Srivastava. Functional data analysis of amplitude and phase variation. *Statistical Science*, 30(4):468–484, 2015.
- Peter Michor, David Mumford, Jayant Shah, and Laurent Younes. A metric on shape space with explicit geodesics. *Atti Accad. Naz. Lincei Cl. Sci. Fis. Mat. Natur. Rend. Lincei (9) Mat. Appl.*, 19, 2007.
- D. Morozov and G. Weber. Distributed merge trees. In *ACM SIGPLAN Notices*, volume 48, pages 93–102. Association for Computing Machinery, NY, 2013.
- Dmitriy Morozov, Kenes Beketayev, and Gunther Weber. Interleaving distance between merge trees. *Discrete & Computational Geometry*, 49:22–45, 2013.
- Hans-Georg Müller. Smooth optimum kernel estimators of densities, regression curves and modes. *The Annals of Statistics*, pages 766–774, 1984.
- Hans-Georg Müller, Ulrich Stadtmüller, and Thomas Schmitt. Bandwidth choice and confidence intervals for derivatives of noisy data. *Biometrika*, 74(4):743–749, 1987.

- Elizbar A Nadaraya. On estimating regression. *Theory of Probability & Its Applications*, 9(1):141–142, 1964.
- Amit Patel. Generalized persistence diagrams. *Journal of Applied and Computational Topology*, 1, 2018.
- Matteo Pegoraro. A persistence-driven edit distance for graphs with abstract weights. *arXiv preprint arXiv:2304.12088*, 2023.
- Matteo Pegoraro. A finitely stable edit distance for merge trees. *arXiv preprint arXiv:2111.02738v5*, 2024a.
- Matteo Pegoraro. A finitely stable edit distance for functions defined on merge trees. *arXiv*, 2108.13108v7 [math.CO], 2024b.
- Florian Pokorny, Majd Hawasly, and Subramanian Ramamoorthy. Topological trajectory classification with filtrations of simplicial complexes and persistent homology. *The International Journal of Robotics Research*, 35(1-3):204–223, 2016.
- Alfio Quarteroni and Alberto Valli. *Numerical approximation of partial differential equations*, volume 23. Springer Science & Business Media, 2008.
- James O. Ramsay and Bernard W. Silverman. *Functional Data Analysis*. Springer, New York, NY, USA, 2005.
- Walter Rudin. Real and complex analysis (mcgraw-hill international editions: Mathematics series). *cit. on*, page 71, 1987.
- L. Sangalli, P. Secchi, and S. Vantini. Analysis of aneurisk65 data: K-mean alignment. *Electronic Journal of Statistics*, 8(2):1891–1904, 2014.
- Laura Sangalli, Piercesare Secchi, Simone Vantini, and Alessandro Veneziani. Efficient estimation of three-dimensional curves and their derivatives by free-knot regression splines, applied to the analysis of inner carotid artery centrelines. *Journal of the Royal Statistical Society Series C*, 58(3):285–306, 2009a.
- Laura Sangalli, Piercesare Secchi, Simone Vantini, and Valeria Vitelli. K-mean alignment for curve clustering. *Computational Statistics & Data Analysis*, 54(5):1219–1233, 2010.
- Laura M. Sangalli, Piercesare Secchi, Simone Vantini, and Alessandro Veneziani. A case study in exploratory functional data analysis: Geometrical features of the internal carotid artery. *Journal of the American Statistical Association*, 104(485):37–48, 2009b.
- E Schuster and S Yakowitz. Contributions to the theory of nonparametric regression, with application to system identification. *The Annals of Statistics*, pages 139–149, 1979.
- Y. Shinagawa, T. L. Kunii, and Y. L. Kergosien. Surface coding based on morse theory. *IEEE Computer Graphics and Applications*, 11(5):66–78, 1991.
- Philip Smith and Vitaliy Kurlin. Families of point sets with identical 1d persistence. 2202.00577 [cs.CG], 2022.
- R. Sridharamurthy, T. B. Masood, A. Kamakshidasan, and V. Natarajan. Edit distance between merge trees. *IEEE Transactions on Visualization and Computer Graphics*, 26(3):1518–1531, 2020.

- A. Srivastava, I. Jermyn, and Shantanu H. Joshi. Riemannian analysis of probability density functions with applications in vision. In *2007 IEEE Conference on Computer Vision and Pattern Recognition*, pages 1–8. IEEE, 2007.
- A. Srivastava, W. Wu, S. Kurtek, E. Klassen, and J. S. Marron. Registration of functional data using fisher-rao metric. *arXiv*, 1103.3817v2[math.ST], 2011a.
- Anuj Srivastava, Eric Klassen, Shantanu Joshi, and Ian Jermyn. Shape analysis of elastic curves in euclidean spaces. *IEEE Transactions on Pattern Analysis and Machine Intelligence*, 33(7):1415–1428, 2011b.
- Charles J Stone. Additive regression and other nonparametric models. *The annals of Statistics*, 13(2):689–705, 1985.
- Elena Farahbakhsh Touli. Frechet-like distances between two merge trees. *ArXiv*, 2004.10747v1[cs.CC], 2020.
- Elena Farahbakhsh Touli and Yusu Wang. Fpt-algorithms for computing gromov-hausdorff and interleaving distances between trees. In *28th Annual European Symposium on Algorithms*, volume 173 of *LIPICs*. Schloss Dagstuhl - Leibniz-Zentrum für Informatik, 2019.
- Simone Vantini. On the definition of phase and amplitude variability in functional data analysis. *Test*, 21(4):1–21, 2009.
- Yuan Wang, Hernando Ombao, and Moo Chung. Topological data analysis of single-trial electroencephalographic signals. *The Annals of Applied Statistics*, 12(3):1506–1534, 2018.
- Kelin Xia, Zhiming Li, and Lin Mu. Multiscale persistent functions for biomolecular structure characterization. *Bulletin of Mathematical Biology*, 80:1–31, 2018.
- Qunqun Yu, Xiaosun Lu, and J. S. Marron. Principal nested spheres for time-warped functional data analysis. *Journal of Computational and Graphical Statistics*, 26(1):144–151, 2013.
- Shanggang Zhou and Douglas A Wolfe. On derivative estimation in spline regression. *Statistica Sinica*, pages 93–108, 2000.
- Yidong Zhou and Hans-Georg Müller. Network regression with graph laplacians. *Journal of Machine Learning Research*, 23(320):1–41, 2022.